

RESEARCH

Open Access



# Repetitive prefrontal tDCS activates VTA dopaminergic neurons, resulting in attenuation of Alzheimer's Disease-like deficits in Tg2576 mice

Maria Luisa De Paolis<sup>1</sup>, Gilda Loffredo<sup>1</sup>, Paraskevi Krashia<sup>2,3</sup>, Livia La Barbera<sup>1,3</sup>, Annalisa Nobili<sup>1,3</sup>, Emma Cauzzi<sup>1</sup>, Lucy Babicola<sup>3,4</sup>, Matteo Di Segni<sup>5</sup>, Roberto Coccorello<sup>3,6</sup>, Stefano Puglisi-Allegra<sup>7</sup>, Emanuele Claudio Latagliata<sup>3,8\*†</sup> and Marcello D'Amelio<sup>1,3\*†</sup>

## Abstract

**Background** Emerging evidence implicates early dysfunction of dopaminergic neurons in the Ventral Tegmental Area (VTA) as a key contributor to Alzheimer's Disease (AD) pathophysiology. Specifically, the VTA dopaminergic neurodegeneration and the consequent reduction of dopamine (DA) in mesocorticolimbic targets are associated with the onset of cognitive impairments and neuropsychiatric-like manifestations in AD animal models. Moreover, decreased midbrain volume and functional VTA disconnection are identified as predictors of accelerated progression from Mild Cognitive Impairment to AD-dementia in clinical populations. Given these findings, interventions capable of directly modulating VTA activity and augmenting DA release, despite the ongoing neurodegeneration, may hold therapeutic potential for mitigating DA-related deficits in AD.

This study aims at evaluating the therapeutic potential of prefrontal transcranial Direct Current Stimulation (tDCS) in the Tg2576 mouse model of AD, exhibiting early VTA dopaminergic neurodegeneration.

**Methods** Repeated tDCS was applied to assess its ability to activate VTA DA neurons. We also evaluated tDCS effects on synaptic plasticity, cognitive and non-cognitive behaviours and AD-related pathology. Hippocampal DA release and Nucleus Accumbens (NAc) DA transporter (DAT) expression were measured. With immunohistochemistry we examined microglial density and morphological complexity at different disease stages. Additionally, intracellular amyloid- $\beta$  (A $\beta$ ) levels and plaque burden were evaluated to determine the impact of tDCS on AD pathology.

**Results** Prefrontal tDCS enhanced the activity of VTA dopaminergic neurons, leading to increased hippocampal DA release and higher DAT levels in the NAc. The enhanced DA outflow is associated with restored CA3-CA1 synaptic plasticity and improvements in recognition memory and motivational behaviours. tDCS reduced microglial numbers and morphological complexity in Tg2576 mice at both pre-plaque stage (7-months) and at an advanced

<sup>†</sup>Emanuele Claudio Latagliata and Marcello D'Amelio contributed equally to this work.

\*Correspondence:

Emanuele Claudio Latagliata  
claudio.latagliata@gmail.com  
Marcello D'Amelio  
m.damelio@unicampus.it

Full list of author information is available at the end of the article



stage characterized by plaque accumulation (12-months). Notably, tDCS also decreased A $\beta$  plaque burden, although no changes in intracellular A $\beta$  levels were observed in younger Tg2576 mice.

**Conclusions** These findings highlight the multifaceted therapeutic potential of prefrontal tDCS in targeting key AD pathophysiological hallmarks, including dopaminergic dysfunction, synaptic impairments, neuroinflammation and plaque deposition. As a non-invasive neuromodulatory approach, prefrontal tDCS emerges as a promising early intervention strategy to complement existing AD treatments, with the potential to improve patient outcomes and quality of life.

**Keywords** Transcranial Direct Current Stimulation, Neuromodulation techniques, Mesocorticolimbic system, Dementia, Hippocampus, Cognitive decline, Neuroinflammation, C-Fos, Transcranial electrical stimulation, Non-Invasive Brain Stimulation

## Background

Alzheimer's Disease (AD) stands as one of the most devastating neurodegenerative disorders of the twenty-first century, characterized by extracellular amyloid- $\beta$  (A $\beta$ ) deposits and intracellular accumulations of hyperphosphorylated tau, which constitute the principal neuropathological criteria for its diagnosis. Clinically, AD is distinguished by the gradual loss of cognitive function and a broad spectrum of neuropsychiatric symptoms (NPS), including apathy, depression and anxiety [1].

Nevertheless, pathological changes associated with AD begin in the brain during the preclinical stage, often decades before the appearance of clinical symptoms [2]. Patients typically progress to Mild Cognitive Impairment (MCI) about 6 to 10 years later, with approximately 15% advancing to dementia within 2 years, and around one-third within 5 years [3]. Thus, focusing on the preclinical and MCI stages is crucial, as early intervention and the management of modifiable risk factors may reduce the risk of onset or delay disease progression.

Mounting evidence suggests a complex pathological landscape of AD, involving multiple neurotransmitter systems. Among these, the dopaminergic mesocorticolimbic circuit—which originates in the Ventral Tegmental Area (VTA) and extensively projects to multiple brain regions including the Prefrontal Cortex (PFC), hippocampus, Nucleus Accumbens (NAc) and amygdala [4]—is gaining a prominent position as it is severely involved in the pathogenesis of the disease, even from its prodromal stages [5–12]. Particularly, clinical studies demonstrated that VTA volume and connectivity correlate with hippocampal function and memory performance in healthy individuals, a relationship that becomes significantly disrupted in MCI and AD patients [13, 14]. In line with this, the mesocorticolimbic areas innervated by the VTA are characterised by hypometabolism and atrophy, and these functional deficits can be predictive for accelerated pathology and faster conversion from MCI to AD dementia [5, 7, 9, 11].

In addition, the involvement of dopaminergic dysfunction in AD not only contributes to cognitive impairments but also leads to NPS manifestations [10, 15, 16]. NPS frequently affect MCI and AD patients and represent significant risk factors for MCI-to-AD conversion, constituting major challenges for patients and caregivers throughout the disease course. Indeed, clinical works studying the functional alterations in mesocorticolimbic targets found a direct correlation between VTA disconnection and NPS in patients since the MCI stage, particularly apathy, anxiety and depression. Moreover, the severity of these symptoms is directly associated to the extent of grey matter loss in mesocorticolimbic targets [5, 7, 10].

These clinical deficits are mirrored in the well-validated Tg2576 mouse model of the disease, bearing the human APP<sub>swe</sub> mutation, which was pivotal in uncovering precocious mechanisms underlying the VTA contribution to AD pathology [16–21]. Indeed, the progressive loss of VTA dopaminergic neurons in Tg2576 mice compromises the functionality of this region, leading to a decrease of DA availability in downstream target areas including the hippocampus and NAc, and consequent synaptic deficits, disruptions in glutamatergic and GABAergic neurotransmission and circuit hyperexcitability. Notably, VTA neurodegeneration in Tg2576 mice precedes amyloid plaque deposition, manifesting as early as 3 months of age, with effects that worsen as the disease advances, further exacerbating its progression. These observations have been further corroborated by findings in other models of AD, reinforcing the broader relevance of VTA dopaminergic dysfunction in AD pathogenesis [22–25].

Importantly, pharmacological interventions targeting the dopaminergic signalling can restore baseline DA levels to control values in critical brain regions, ameliorating synaptic plasticity deficits, cognitive decline and behavioural impairments in both preclinical studies [16, 17, 26–34] and AD patients [35–38]. Such findings, combined with evidence highlighting DA's pivotal role in modulating hippocampal plasticity [39–41] and its

protective effects against neuroinflammation [42–45] and amyloid plaque formation [46–49], emphasize the dopaminergic system as a critical therapeutic target in AD and support the hypothesis that interventions aimed at restoring DA signalling could have widespread benefits.

In this context, transcranial Direct Current Stimulation (tDCS) emerges as a promising therapeutic approach. This non-invasive and versatile neuromodulatory technique delivers low-intensity electrical currents through scalp electrodes, inducing lasting changes in neuronal excitability and synaptic plasticity [50, 51]. The mechanisms underlying tDCS effects are multifaceted, involving modulation of neurotransmitter systems, regulation of NMDA receptor activity, BDNF expression, balancing excitatory and inhibitory neurotransmission and promoting structural and functional connectivity changes [52–55]. Furthermore, tDCS exhibits significant anti-inflammatory properties, reducing microglial activation and pro-inflammatory cytokine production [56, 57]. Even more critical is the ability of prefrontal tDCS to reach and activate subcortical deep brain structures, such as the VTA and associated mesencephalic areas. Specifically, in both non-AD rodent models and humans, prefrontal tDCS showed significant potential in modulating dopaminergic neurotransmission, including increased DA release in striatal regions and improved cognitive and motivation-related behaviours. Thus, the modulation of the mesocorticolimbic pathway may be a possible mechanism of action underlying prefrontal tDCS-induced changes in subcortical DA regions [58–70]. However, whether prefrontal tDCS can activate the VTA during the ongoing degeneration that characterizes the AD brain remains unexplored with clinically relevant implications for personalized treatments.

Here, we sought to investigate this aspect in Tg2576 mice, by conducting a two-week stimulation protocol of anodal prefrontal tDCS at two key ages, 7 and 12 months. The 7 months age point represents a pre-plaque stage, while 12 months reflect a more advanced disease state, with significant hippocampal A $\beta$  plaque accumulation. Using two different stages helped us to evaluate distinct pathological events within the progression of AD symptoms. Our results prove that prefrontal tDCS induces a selective activation of the remaining VTA dopaminergic neurons, enhancing DA outflow and, as a result, restoring hippocampal and NAc functionality. Additionally, we demonstrate that prefrontal tDCS blunts microglia-mediated neuroinflammation and reduces amyloid pathology.

Our findings provide crucial insights for optimizing tDCS protocols and establishing this technique as a viable therapeutic option that can be integrated into the intervention of both early- and late-stage of AD. By exploring the early involvement of the dopaminergic

system and leveraging the unique capabilities of tDCS in neuromodulation, this work paves the way for innovative treatment strategies aimed at positively modifying the disease trajectory.

## Methods

### Animals

Heterozygous male and female Tg2576 mice [71] (APP-SWE—Model #1349 TACONIC) and Wild-Type (WT) littermates were used at 7- and 12-months of age, as described in the text. Animals were housed with ad libitum food and water, with a 12-h light/dark cycle. All experimental procedures complied with the ARRIVE guidelines and were carried out in accordance with the ethical guidelines of the European Council Directive (2010/63/EU).

### Surgical implantation of epicranial cannula and prefrontal tDCS stimulation protocol

Implantation of a prefrontal epicranial cannula was performed 2 days before starting the stimulation sessions. Mice were anesthetized with a combination of Rompun (20 mg/mL, 0.5 mL/kg; Bayer) and Zoletil (100 mg/mL, 0.5 mL/kg; Virbac; intraperitoneally) before the surgical procedure. The animals were then placed under a stereotaxic apparatus and a small incision was made in the skin of the head. After skull exposure and cleaning, a plastic tubular cannula (2.5 mm diameter) was implanted on the midline under stereotaxic control (David Kopf Instruments) over the PFC (AP: +3.2 from bregma). To secure the cannula to the skull at the desired position, we first used instant glue to fix it firmly, followed by a thin layer of non-toxic glass ionomer cement (GlasIonomer Cement CX-Plus Kit; Shofu Inc.). To ensure an uninterrupted current flow during stimulation, the inside of the tubular cannula was left free of cement; additionally, to prevent debris/sawdust accumulation, the cannula was filled with soft cotton between experimental sessions. At the end of the procedure, animals were placed on a heated pad to maintain stable body temperature until fully awakened. Upon complete awakening, animals were housed individually to prevent inadvertent implant removal by conspecifics.

After the post-surgical recovery period, mice were randomly assigned to one of the four experimental groups (WT Sham, WT tDCS, Tg Sham and Tg tDCS). The animals then underwent 10 sessions of prefrontal tDCS or Sham stimulation (5 days per week, with a 2-day break between sessions for a total ten days of stimulation; Fig. 1a). To avoid potential confounding effects related to anaesthesia, animals were awake throughout the stimulation procedure. Animals were fitted with a custom-made Velcro jacket, securely fastened with a metal clip. The

jacket contained a sponge pocket filled with conductive gel (ECI Electro-Cap Electro-Gel, Neuroevolution—Sistemas Médicos, Lda). The same gel was also applied to the inner surface of the prefrontal cannula implanted during surgery to facilitate stable electrode placement and signal conductance. Animals were then restrained in plexiglas holders to maintain consistent positioning during the stimulation session.

Stimulation was administered using a device (DC-Stimulator Plus, NeuroConn, Germany) with the anodal (active) electrode positioned in the prefrontal cannula and the cathodal (reference) electrode in the gel-filled pocket on the jacket. Both tDCS and Sham-treated mice underwent identical handling protocols, with the tDCS group receiving a continuous DC of 25  $\mu\text{A}$  for 20 min per session, while Sham animals were connected to the stimulator without current flow. The stimulation parameters were selected to yield a current density of  $\sim 0.51 \text{ mA/cm}^2$ , considering an electrode surface of  $4.91 \text{ mm}^2$  [72]. The applied current reflects a compromise between translational relevance and experimental safety, being well below standard preclinical intensities (e.g., 200  $\mu\text{A}$ ) and avoiding the risk of tissue damage in mice. In line with this, recent *in vivo* work demonstrated that electric fields in the range of 0.35–1 V/m—equivalent to low-intensity tDCS—are sufficient to modulate the firing rate of hippocampal neurons in awake rodents [73]. To avoid painful current transitions, controlled DC ramp-up and ramp-down phases were also implemented by setting fade-in and fade-out to 20 s values. After each stimulation session, animals were promptly returned to their home cages, where they remained for an additional 1–2 days, depending on the subsequent experimental protocol.

For the analysis of c-Fos expression, the stimulation protocol involved a single prefrontal tDCS session

administered under isoflurane anaesthesia, thereby obviating the need for animal restraint on the plexiglass support. Anaesthesia was induced with 2–3% isoflurane, maintained at 0.8–1.5%, with an oxygen flow of 1.6–1.8 L/min. Animals were sacrificed one hour after the stimulation session.

#### In vivo microdialysis and Ultra-Performance Liquid Chromatography (UPLC)

To evaluate hippocampal DA and norepinephrine (NE) levels, mice were prepared for microdialysis through unilateral probe implantation, conducted the last day of tDCS. Mice were anaesthetized with Zoletil and Rompun, then secured in a stereotaxic apparatus to vertically implant a concentric microdialysis probe (AN69 fibres, Hospal Dasco) targeted at the hippocampus (AP:  $-3.0$ , ML:  $\pm 3.0$  mm from bregma) with a total length of 5 mm (of which 3 mm consisted of the dialysis membrane; Fig. 1c). After probe placement, the surgical area was sutured and animals were returned to individual housing. To ensure stability and protection of probe connections, the inlet and outlet tubing of the probe were connected to two PE-20 segments (1–1.5 cm each) via flexible swivels.

Membrane recovery efficiency was validated *in vitro* prior to implantation to warrant consistent sampling. On the day of the experiment, 2 days after recovery from tDCS or Sham stimulation, the animal was placed in a circular cage filled with bedding, and the probe was connected to the microdialysis system, allowing the animal to move freely. Specifically, the small PE-20 tubing segments initially attached to the microdialysis probe's inlet and outlet were removed and replaced with longer PE-20 tubing. These extended segments were then connected to the CMA/100 microinfusion pump (Carnegie Medicine) via an ultra-low torque multichannel swivel (MCS5 model, Instech Laboratories), providing continuous

(See figure on next page.)

**Fig. 1** Prefrontal tDCS enhances hippocampal DA outflow *via* activation of VTA neurons in 7-month-old Tg2576 mice. **a** Schematic representation of the experimental timeline: Tg2576 and WT mice (7- or 12-month-old) were implanted with prefrontal cannulae, followed by a 2-day recovery period. Mice then received either daily tDCS (20 min/day, 5 days/week) or Sham stimulation for two consecutive weeks (for c-Fos analysis, a single session of tDCS or Sham stimulation was administered under isoflurane anaesthesia, and 7-month-old animals were sacrificed 1 hour post-stimulation). After 2 more days of recovery, 7-month-old mice underwent subsequent behavioural or neurophysiological experiments. 12-month-old mice were used only for neuroinflammation and plaque analysis. **b** Representative coronal section and confocal images of the VTA (upper panel) and LC (bottom panel) showing c-Fos (red) labelled nuclei of TH<sup>+</sup> neurons (green) of 7-month-old Tg Sham and Tg tDCS mice (scale bar: 10  $\mu\text{m}$ ). Plots show the percentage of c-Fos<sup>+</sup>/TH<sup>+</sup> neurons within the VTA or the LC ( $n = 3$  mice/group; VTA: unpaired *t*-test: \*\* $p = 0.0047$ ). **c–e** Schematic representation of *in vivo* microdialysis setup for measuring neurotransmitter release. Plots show basal and KCl-induced hippocampal DA (d) and NE (e) levels in 7-month-old WT Sham ( $n = 4$  males), WT tDCS ( $n = 4$  males), Tg Sham ( $n = 4$  males) and Tg tDCS ( $n = 6$  males) mice measured at different time points (mean  $\pm$  S.E.M.; d, 3-way RM-ANOVA: time  $\times$  genotype  $\times$  treatment,  $F_{4,56} = 0.7572$ ,  $p = 0.5575$ ; time,  $F_{4,56} = 16.60$ ,  $p < 0.0001$ ; genotype,  $F_{1,14} = 1.608$ ,  $p = 0.2254$ ; treatment,  $F_{1,14} = 4.785$ ,  $p = 0.0462$ ; Tg Sham Post KCl 1–Tg tDCS Post KCl 1 \*\* $p = 0.0014$ , WT tDCS Basal Mean–WT tDCS Post KCl 1  $p = 0.0059$ , Tg tDCS Basal Mean–Tg tDCS Post KCl 1  $p < 0.0001$  all with Tukey's post hoc test. e, 3-way RM-ANOVA: time  $\times$  genotype  $\times$  treatment,  $F_{4,48} = 0.1822$ ,  $p = 0.9465$ ; time,  $F_{4,48} = 26.24$ ,  $p < 0.0001$ ; genotype,  $F_{1,12} = 0.1302$ ,  $p = 0.7245$ ; treatment,  $F_{1,12} = 0.0500$ ,  $p = 0.8268$ ; Tg Sham Basal Mean–Tg Sham KCl  $p = 0.0118$ , Tg tDCS Basal Mean–Tg tDCS KCl  $p = 0.0003$  both with Tukey's post hoc test). In all figures, empty dots refer to female mice, while full dots to males. [Figure created using BioRender.com]

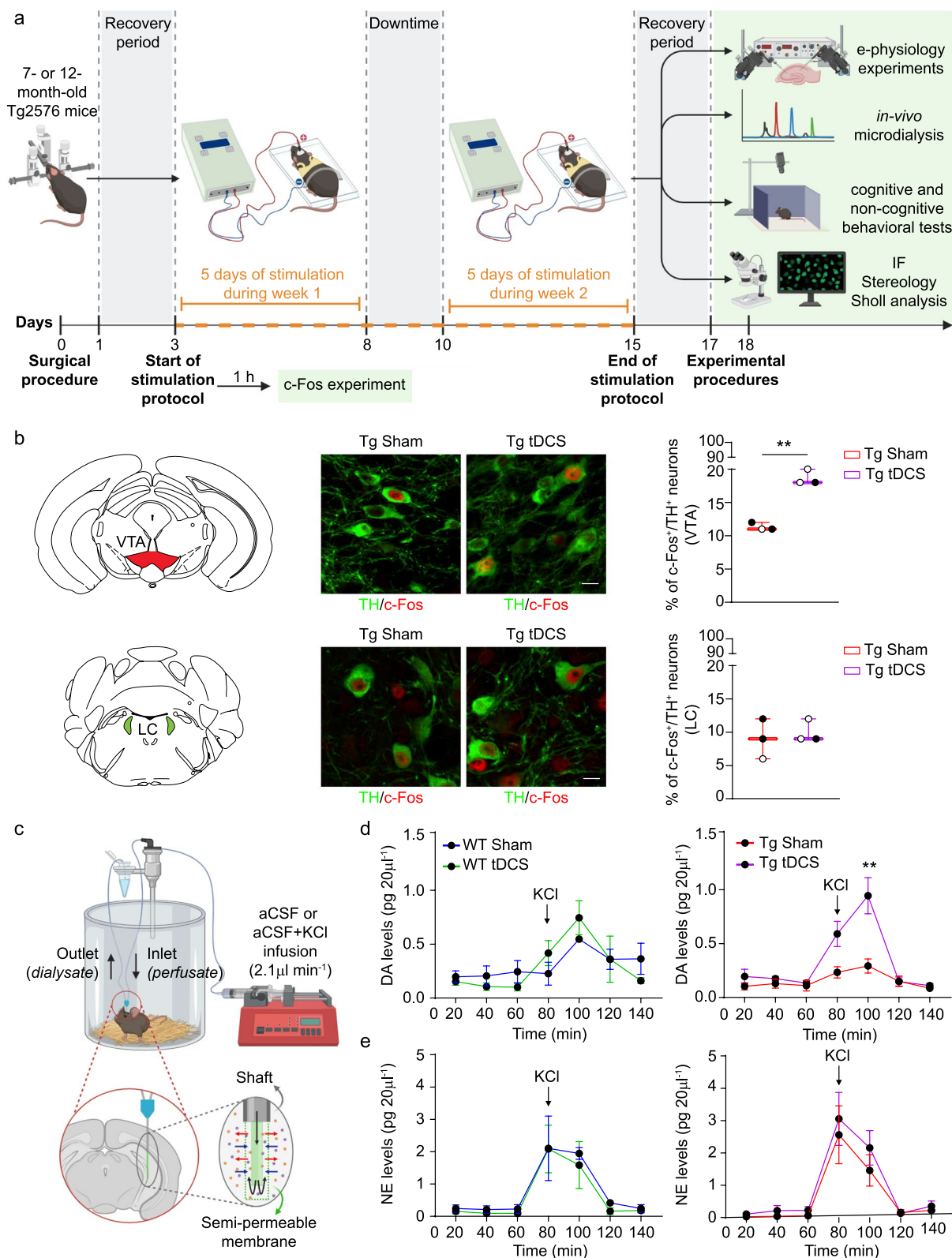


**Fig. 1** (See legend on previous page.)

perfusion of the probe during the experiment. A steady infusion of artificial cerebrospinal fluid (aCSF; in mM: NaCl 140, KCl 4, CaCl<sub>2</sub> 1.2, MgCl<sub>2</sub> 1) was maintained through the probe at a rate of 2.1 µL/min. After initiating perfusion, animals were allowed to acclimate for 1 h to establish a stable baseline. Three consecutive baseline samples were then collected at 20-min intervals over a 60-min period in tubes containing antioxidant solution containing 100 mM acetic acid, 3.3 mM L-cysteine, 0.27 mM Na<sub>2</sub>EDTA and 12.5 µM. Baseline collection was followed by a 20-min perfusion with KCl-enriched aCSF solution (100 mM KCl) to induce depolarization and neurotransmitter release, after which a single dialysate sample was collected. The perfusion was then switched back to aCSF, and three additional samples (Post KCl 1, 2 and 3) were collected over the next hour.

To verify probe placement, brains were postfixed in 4% paraformaldehyde, sectioned coronally (100 µm), stained with methylene blue and then examined under a microscope. Data from animals with improperly allocated probes were excluded from subsequent analyses.

Dialysate samples (20 µL) were analysed via an UPLC system (ACQUITY, Waters Corporation) equipped with an amperometric detector (Decade II, Antec Leyden). The UPLC system consisted of an electrochemical flow-cell (VT-03, Antec Leyden) with a 0.7 mm glassy carbon working electrode, maintained at a potential of 400 mV, and an in-situ Ag/AgCl reference electrode. The flow cell was positioned downstream of a BEH C18 column (2.1 × 50 mm, 1.7 µm particle size; Waters Corporation) kept at 37 °C with a mobile phase flow rate of 0.07 mL/min. The mobile phase composition was (in mM): 50 orthophosphoric acid 85%, 8 KCl, 0.1 EDTA, 2.5 1-octanesulfonic acid sodium salt, 14% methanol, adjusted to pH 6.03 with NaOH. DA and NE peak heights were identified by comparison with standards containing the antioxidant solution as above. For in vivo microdialysis experiments, only male mice were used to avoid the potential confounding effects of hormonal fluctuations across the oestrous cycle [74–76].

#### Acute brain slicing and electrophysiological recordings

Acute brain slices for electrophysiological recordings were obtained following the protocol outlined in [77]. Briefly, solutions for brain slicing were prepared fresh (stored at +4 °C for up to 5 days) and saturated with a 95% O<sub>2</sub> and 5% CO<sub>2</sub> mixture before use. Animals were anaesthetized with halothane and then transcatheterially perfused with cold (0–2 °C) oxygenated solution containing (in mM): 92 NMDG, 2.5 KCl, 1.25 NaH<sub>2</sub>PO<sub>4</sub>, 30 NaHCO<sub>3</sub>, 20 HEPES, 25 Glucose, 2 Thiourea, 5 Na-Ascorbate, 3 Na-Pyruvate, 0.5 CaCl<sub>2</sub> and 10 MgSO<sub>4</sub> (~ 295 mOsm; pH 7.3–7.4 with 5 M HCl). Afterwards, the

animal was decapitated, the brain was rapidly removed and parasagittal brain slices containing the dorsal hippocampus (300 µm thickness) were cut with a vibratome (VT1200S, Leica) in the same chilled-bubbled perfusion solution. After slicing, slices were transferred to a holding chamber containing the NMDG-based solution at 32–34 °C and left to recover for 35 min, during which NaCl, prepared fresh on the experimental day, was added gradually to the solution at 5-min intervals. Subsequently, slices were transferred at room temperature to a long-term holding chamber containing (in mM): NaCl 92, KCl 2.5, NaH<sub>2</sub>PO<sub>4</sub> 1.25, NaHCO<sub>3</sub> 30, HEPES 20, Glucose 25, Thiourea 2, Na-Ascorbate 5, Na-Pyruvate 3, CaCl<sub>2</sub> 2 and MgSO<sub>4</sub> 2 (~ 300–310 mOsm; pH 7.3–7.4 with NaOH 10 N) for at least 1 h before experiments. In this last solution, slices remained for the entire experimental day.

#### Multielectrode array recordings

A single acute slice containing the dorsal hippocampus was transferred onto an 8 × 8 array of planar multielectrodes, each 50 × 50 µm in size with an interpolar distance of 150 µm (MED-P5155, Alpha MED Sciences). Slice position and contact with electrodes was secured by a nylon mesh glued to a flattened piece of platinum wire. The brain slice was continuously perfused with oxygenated aCSF solution containing (in mM): NaCl 124, KCl 3, NaH<sub>2</sub>PO<sub>4</sub> 1.25, 26 NaHCO<sub>3</sub>, 10 Glucose, 1 MgSO<sub>4</sub>, 2 CaCl<sub>2</sub>, and 0.5 mM L-glutamine (10 mL/min, 32–34 °C). The brain slice was visualized at 2.5x magnification of an upright microscope (Leica DM-LFS, Leica Microsystems), while raw data were recorded with the MED64 System (Alpha MED Sciences), digitized at 20 kHz with a 6071E Data Acquisition Card (National Instruments), and low-cut filtered at 1 Hz. Amplitude, duration, and frequency of stimulation were controlled by Mobius software (Alpha MED Sciences).

In order to record *field* excitatory postsynaptic potentials (*fEPSPs*), Schaffer collateral stimulation was performed (200 µs duration), after choosing one stimulation electrode in the Stratum Radiatum and another recording electrode in the pyramidal cell layer in CA1 area, maintaining a constant distance between electrodes of 300 µm. After at least 20–30 min of baseline stable responses (single half-maximal stimulus, every 30 s), Long-Term Potentiation (LTP) was induced, by applying two conditioning trains of 100 Hz stimuli for 1 s administered at an interval of 20 s, followed by test stimulation for at least 1 h. The magnitude of LTP was assessed by calculating the mean peak of *fEPSP* during the final 5 min following the high-frequency trains, normalized to the mean baseline peak. All recordings obtained were analysed using Mobius (Alpha MED Sciences) and Origin6.0 (Microcal Software Inc.) software.

### Behavioural testing

All behavioural assessments were conducted 2 days following the completion of the tDCS sessions (Fig. 1a). Before each session, subjects were acclimated in an adjacent room where ambient lighting (15 lx) and noise levels (35 dB) were matched to those of the experimental environment. These environmental conditions were kept constant throughout all phases of testing. To minimize olfactory cues from influencing the mice's exploration patterns, all experimental apparatus, including objects used for object recognition, were thoroughly cleaned with 5% ethanol between sessions and experimental subjects.

### Open field and Novel Object Recognition (NOR) tests

The experimental protocol commenced with the open field test, conducted over two consecutive days to assess locomotor activity in a circular arena (60 cm in diameter, 40 cm in height), made of plexiglass with a white base and opaque grey walls. On Day 1, each mouse was positioned at a fixed starting point near the arena's edge and allowed to freely explore for 10 min. The same procedure was repeated on Day 2. Data on locomotor activity were provided only by the test conducted on Day 1, but the dual-day exploration served as pre-habituation for the subsequent NOR test, ensuring that the animals were adequately familiarized with the environment.

On Day 3, the NOR test was performed in the same open field arena. The training phase began with the placement of two identical wooden spheres within the arena, positioned equidistant from the arena centre. Mice were allowed to explore for 10 min. After a 24-h interval (Day 4), each mouse was reintroduced to the arena for a 10-min testing phase, during which one of the wooden spheres was replaced with a metal column of similar size. The spatial configuration of the objects remained identical to that of the training phase, with the novel object positioned on alternating sides to control for potential side bias.

In both the open field and NOR test, exploratory behaviour was recorded using VirtualDub software (version 1.10.4), which tracked the mouse's movements and interactions with the objects. Behaviour analysis for the open field test was performed using ImageJ software (version 1.53q; National Institute of Health, USA; <http://imagej.nih.gov/ij/>), allowing for the tracking of the total distance travelled (in cm) by each animal in the arena, recorded on the experimental Day 1. For the NOR test, data were analysed using the free, open-source software BORIS (version 8.21.10; University of Torino, Italy; [78]), which provided the total exploration time (in s) spent on each object. Exploration was defined as any interaction

with the object, including touching it with the nose or forepaws, climbing on it, or sniffing within a 2 cm radius.

### Tail Suspension Test (TST)

A separate cohort of animals, distinct from those used in other behavioural assays, was employed for the TST. The apparatus consisted of a rectangular wooden base (20 × 15 cm) with three perpendicular vertical wooden walls. A rectangular metal bar, securely affixed to the top of the apparatus, was utilized for suspending the mice by their tails during the experiment. Prior to testing, each subject's tail was carefully inserted into a black plexiglass cylinder to prevent tail-climbing behaviour, which could confound test results. Subsequently, a strip of paper tape was applied to the tail approximately 3 mm from the distal end, ensuring a secure attachment to the metal bar at the top of the apparatus. During the test, each mouse was suspended approximately 20 cm above the base of the apparatus for a total of 6 min. The experimental session was continuously recorded with VirtualDub and data were analysed with BORIS to assess the duration time (in s) of both immobility, classified as passive behaviour and defined as a complete lack of movement except for minor adjustments to maintain balance, and active behaviour, encompassing all movements aimed at escape or repositioning (such as limb movements and attempts to reach the bar). At the end of the session, the paper tape and cylinder were carefully removed, and each subject was gently returned to its home cage. Each subject underwent testing individually to avoid potential influence from other animals.

### Immunofluorescence

Following anaesthesia (Rompun/Zoletil), mice were transcardially perfused with Phosphate Buffer (PB; 0.1 M, pH 7.4) and 4% paraformaldehyde in PB. After isolation, brains were postfixed in 4% paraformaldehyde for at least 4 h, dehydrated and cryoprotected in 30% sucrose in PB at 4 °C until sinking. Coronal sections (30 µm-thick) were cut with a cryostat and slices were collected in PB-Sodium Azide 0.02% until experiments.

Free floating slices were incubated with primary antibodies in PB containing 0.3% Triton X-100 overnight at 4 °C. For DAT levels free floating sections were incubated with primary antibody in permeabilization solution for 3 nights at 4 °C. For Aβ/Iba1 immunostaining, sections were pretreated with M.O.M.<sup>®</sup> (Mouse on Mouse) Blocking Reagent (1:1000; Vector laboratories, #MKB-2213-1, 2 h, RT) diluted in permeabilization solution (PB with 0.3% Triton X-100), and then incubated with primary antibodies overnight at 4 °C in permeabilization solution. Sections were subsequently washed in PB and incubated with secondary antibodies in the permeabilization

solution (2 h, RT) followed by washes in PB and incubation with DAPI (1:1000, Serva). After mounted, slices were examined using a Nikon Eclipse Ti2 confocal microscope. The labelling specificity was confirmed by omission of primary antibodies and use of normal serum instead (negative controls).

For all analyses, images were acquired with 10x or 20x-objectives by performing Z-stacks, then processed by maximum-intensity projection.

For the quantitative analysis, images were processed simultaneously and analysed with ImageJ: after 8-bit conversion and background subtraction, the signal was quantified by measuring the relative fluorescence intensity. The F/A ratio defines mean fluorescence intensity (F) over a defined surface area (A). All samples were captured with identical Z-stack thickness and laser settings.

Levels of intracellular A $\beta$  and striatal DAT were quantified by setting 10 randomly distributed squared frames (70  $\times$  70 pixel).

The mean number of A $\beta$  plaques in the hippocampus was quantified manually from 10x-objective images.

The mean number of c-Fos<sup>+</sup>/Tyrosine Hydroxylase<sup>+</sup> (TH<sup>+</sup>) neurons over the defined area captured by the camera was quantified by using NIS-Elements software (Nikon<sup>®</sup> Instruments Inc.).

Images were collected and quantification was done at least on 3–4 slices per mouse. Data were then averaged per mouse for figures and statistical analysis. Exclusively for the representative confocal images, after the quantitative analysis, LUTs were equally increased at the same level for all groups of a given experiment. Quantitative analyses were performed on raw images.

Primary antibodies: c-Fos (1:1000, Abcam #ab190289; RRID:AB\_2737414), DAT (1:400; Chemicon; #MAB369; RRID:AB\_2190413), hAPP695 (6E10; 1:500, BioLegend #803001; RRID:AB\_2564653), IBA1 (1:600; Wako #019–19741; RRID:AB\_839504), TH (1:1000; Millipore #MAB318; RRID:AB\_2201528).

Secondary Antibodies (Thermo Fisher Scientific): Alexa Fluor-555 donkey anti-rabbit (1:200; #A31572; RRID:AB\_162543), Alexa Fluor-488 donkey anti-mouse (1:200; #R37114; RRID:AB\_2556542), Alexa Fluor-647 donkey anti-mouse (1:200; #A31571; RRID:AB\_162542), Alexa Fluor-555 goat anti-rat (1:200; #A48270; RRID:AB\_2535855).

### Stereology

Immunofluorescence sections were used to estimate microglia cell numbers in the dorsal hippocampus, outlined using the 5x-objective; Iba1<sup>+</sup> cells were marked with a 40x-objective (x, y, z dimension of probe was 100  $\times$  100  $\times$  25  $\mu$ m). The total cell number was estimated according to the formula (Eq. 1):

$$N = SQ \times (1/ssf) \times (1/asf) \times (1/tsf) \quad (1)$$

where SQ represents the neuron number counted in all optically sampled fields of the ROI, *ssf* is the section sampling fraction, *asf* is the area sampling fraction and *tsf* is the thickness sampling fraction.

### Sholl analysis

For quantitative 3D-analysis of the entire cell, including soma and perimeter, microglia were imaged with a Zeiss Microscope (Axio Imager KMAT) with a motorized stage and a camera controlled by the Neurolucida software (7.5v; MBF Bioscience) [79]. We examined only non-overlapping cells with clear soma and branching. Sholl analysis included counting the number of dendritic intersections, nodes and endings, and the lengths of processes at fixed distances from the soma in 10  $\mu$ m-distanced concentric circles away from the soma. Analysis was done with a 100x-oil objective. Nine representative cells/animal were randomly analysed, and data were averaged for each mouse.

### Power analysis, sample size, randomization, blinding

The number of experimental units per group and experiment was determined with power analysis (G\*Power software, version 3.1.9.7) using a power of 0.8 and errors of 0.05; standard deviations were obtained from our previous publications [16, 19]. Comprehensive power analysis parameters supporting the determination of sample size are provided in Additional Table S1.

To decide how mice from the same litter would be “destined” to different groups, we randomized animals using with a random-number table.

All researchers were blinded to the animal group and un-blinding occurred only after analysis.

Details for the experimental units for each experiment are described in figure legends.

### Statistical analysis

Statistical analyses were conducted using Prism software (version 8.01; GraphPad). Data distribution was assessed for normality utilizing the Shapiro–Wilk, Kolmogorov–Smirnov or D’Agostino & Pearson tests.

Comparisons between two experimental groups (e.g., Tg Sham vs. Tg tDCS) were performed using 2-tailed parametric tests (unpaired *t*-test or Welch’s *t*-test) for data meeting the assumptions of Gaussian distribution, and non-parametric Mann–Whitney test for data that did not meet normality criteria. For datasets involving paired measurements, such as the training and testing phases of the NOR test, paired *t*-tests were used for normally distributed data, or Wilcoxon matched-pairs signed rank tests otherwise.

Analyses involving comparisons among more than two groups (e.g., WT Sham, WT tDCS, Tg Sham, Tg tDCS) were performed using 2-way Repeated-Measures ANOVA, followed by Tukey's or Sidak's multiple comparison post hoc tests. If no significant interaction was observed between the independent variables, statistical comparisons were conducted using *t*-tests.

Microdialysis data (analysed with genotype, treatment and dialysis time point—baseline, KCl, post-KCl—as independent factors) were evaluated using 3-way Repeated-Measures ANOVA with Tukey's multiple comparison post hoc tests for further pairwise comparisons.

Statistical significance was defined as  $p \leq 0.05$ . In box-and-whisker plots, the central line represents the median, the box edges indicate the upper and lower quartiles, whiskers show minimum and maximum values and points represent individual experiments. Sex distribution for each experimental group is reported in figure legends (empty dots refer to female mice, while full dots to males). All other data are presented as mean  $\pm$  S.E.M. For additional details on statistical analyses and sample sizes, please refer to figure legends.

## Results

### Prefrontal tDCS activates DA neurons in the VTA and enhances DA release in Tg2576 mice

Previously, we demonstrated that the AD mouse model Tg2576 experiences progressive and selective degeneration of DA neurons in the VTA beginning at 3 months of age [16]. This degeneration is linked to numerous neuronal dysfunctions and synaptic deficits, leading to behavioural impairments observable since the pre-plaque stage [17, 20, 21].

Our initial objective was to evaluate the efficacy of prefrontal tDCS in stimulating the surviving dopaminergic neurons in the VTA of Tg2576 mice. To this end, 7-month-old Tg2576 mice underwent either prefrontal tDCS (referred to as Tg tDCS) or Sham stimulation (Tg Sham) under isoflurane anaesthesia, as described in the Methods section (Fig. 1a). One hour after delivering a single prefrontal tDCS session, we performed immunofluorescence analyses for c-Fos expression—an immediate-early gene commonly used as a marker of neuronal activation. We observed a significant increase in the number of c-Fos<sup>+</sup>/TH<sup>+</sup> neurons in the VTA of Tg tDCS mice compared to Tg Sham mice, indicating that prefrontal tDCS robustly activates DA neurons (Fig. 1b, *upper panel*). We extended our analysis to the noradrenergic Locus Coeruleus (LC), another brainstem nucleus co-releasing DA and primarily affected in AD [80–82]. In contrast to what we observed in VTA, the LC showed no modifications in the number of activated neurons

following prefrontal tDCS, indicating that this region is not modulated by the stimulation (Fig. 1b, *bottom panel*).

We next examined whether repeated sessions of prefrontal tDCS could modulate hippocampal dopaminergic signalling in freely moving Tg2576 mice and age-matched WT littermates. After two weeks of prefrontal tDCS or Sham treatment (Fig. 1a), through *in vivo* microdialysis we measured hippocampal DA levels evoked by extracellular KCl (Fig. 1c). No changes were observed in WT mice that underwent tDCS (WT tDCS; Fig. 1d, *left panel*). In contrast, Tg tDCS mice exhibited significantly higher levels of hippocampal DA outflow compared to Tg Sham mice (Fig. 1d, *right panel*). Of note, hippocampal NE levels were unaffected across all experimental groups (Fig. 1e), consistent with c-Fos data showing the lack of LC activation by tDCS.

Collectively, these results prove that prefrontal tDCS elicits an increase in evoked hippocampal DA outflow in Tg2576 mice through targeted activation of VTA DA neurons, suggesting that this stimulation can effectively stimulate dopaminergic pathways known to be impaired in AD.

### Restoration of synaptic plasticity in CA3-CA1 synapses of Tg2576 mice following prefrontal tDCS

The dopaminergic signalling from the VTA is critical for hippocampal-dependent memory formation and LTP, increasing synaptic strength in response to activity patterns or motivational demands [40, 41]. Indeed, we previously showed that many hippocampal deficits in neuronal function and behaviours can be restored by brief DA-based pharmacological treatments [16, 17, 20]. Given the observed increase in hippocampal DA levels in Tg2576 mice following prefrontal tDCS, we next wondered whether this could be translated into functional improvements in LTP in the CA3-CA1 hippocampal pathway.

We confirmed that 7-month-old Tg Sham mice exhibited significant impairments in CA3-CA1 LTP compared to WT Sham mice. Importantly, prefrontal tDCS promoted a full restoration of LTP in Tg tDCS mice, comparable to the levels of WT Sham mice (Fig. 2). The rescue of synaptic plasticity deficit in Tg2576 mice suggests that prefrontal tDCS may counteract AD-related defects in hippocampal function.

### Prefrontal tDCS restores cognitive and non-cognitive deficits in Tg2576 mice

DA release in the hippocampus promotes object recognition and spatial memory, reward-associated memory, and memory consolidation [40, 80, 82–86]. Thus, considering the enhanced hippocampal DA levels and the rescue of hippocampal synaptic plasticity after prefrontal tDCS, we next sought to determine whether the tDCS-mediated

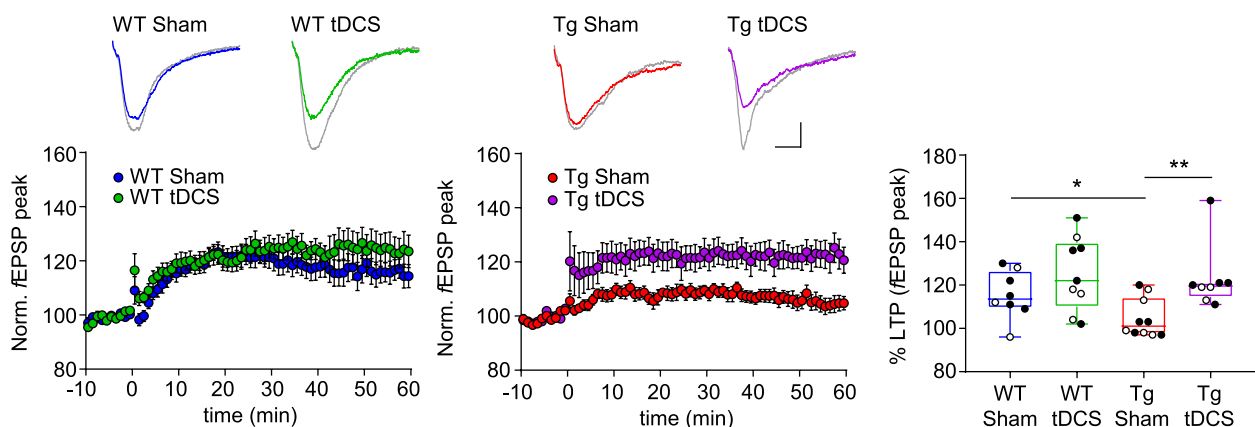


**Fig. 2** Prefrontal tDCS rescues synaptic plasticity in 7-month-old Tg2576 mice. Time-course plots showing LTP at CA3-CA1 synapses in acute hippocampal slices from 7-month-old Tg2576 and WT mice following tDCS or Sham treatment. Each plot presents the normalized average fEPSP peak amplitude (mean  $\pm$  S.E.M) recorded in the CA1 region, with an initial 10-min baseline period, after which a HFS was applied to the Schaffer collateral pathway in CA3. Above are representative traces (scale bar: 0.1 mV; 0.5 s) illustrating fEPSPs at half-maximum stimulation recorded during baseline (coloured trace) and at 1-h post-conditioning stimulus (grey trace). Box-and-whisker plot shows the percentage of potentiation measured 60 min post-HFS (WT Sham:  $n = 8$  slices/3 mice; WT tDCS:  $n = 9$  slices/4 mice; Tg Sham:  $n = 10$  slices/6 mice; Tg tDCS:  $n = 8$  slices/4 mice; WT Sham–Tg Sham  $*p = 0.0368$  with 2-tailed unpaired  $t$ -test; Tg Sham–Tg tDCS  $**p = 0.0028$  with Mann–Whitney test)

neuromodulation of the dopaminergic drive could be translated into cognitive and/or non-cognitive improvements in 7-month-old Tg2576 mice. We first focused on object recognition memory, a core domain of declarative memory often compromised in Tg2576 mice [87, 88] that can be prevented by reducing the VTA DA neurodegeneration [19]. During the training phase of the NOR test, no significant differences were observed in exploration times for the two identical objects across all groups (Fig. S1), confirming an unbiased baseline for object preference. During the testing phase (24 h after training), both WT Sham and WT tDCS groups showed a robust preference for the novel object, whereas Tg Sham mice did not display differential exploration between the two objects, confirming an impairment in recognition memory. Importantly, Tg tDCS mice behaved similarly to both WT groups, showing significantly higher exploration of the novel object compared to the familiar one, as an index of the restored recognition memory (Fig. 3a).

Based on the known role of DA in driving motivation and reward via the VTA-NAc pathway, and the fact that the VTA takes part in locomotion in novel environments [89], we tested mice's locomotor activity and depressive-like state through the open field test and TST, dysregulated in Tg2576 mice [90]. In the open field test, Tg Sham mice demonstrated increased locomotor activity, covering a significantly greater distance compared to WT controls. However, prefrontal tDCS treatment normalized the locomotor behaviour in Tg mice, reducing the total distance travelled (Fig. 3b). In

the TST, unexpectedly Tg Sham mice showed no differences in both passive and active behaviours when compared with WT controls (Fig. 3c), indicating an apparent lack of depressive-like behaviours. This result may be attributable to the hyperlocomotion observed in this model (Fig. 3b), which could mask potential depressive-like immobility in this test. Instead, tDCS-treated Tg mice exhibited a strong reduction in immobility time and an increase in active movements compared to Tg Sham mice (Fig. 3c). Considering the reduced locomotor activity observed in Tg tDCS mice in the open field test, the increased active behaviours in the TST likely reflect a genuine improvement in motivation rather than an exacerbation of hyperactivity. To reinforce this hypothesis, we examined dopaminergic fibres in NAc core and shell regions. As expected, Tg Sham mice showed a strong reduction in DAT levels compared to WT animals in both NAc regions (Fig. S2), mirroring the reduction in DA levels in naïve Tg2576 mice [16, 18]. Importantly, the prefrontal tDCS induced an increase in DAT levels in both NAc subregions of Tg tDCS mice, in line with an enhancement of the dopaminergic drive to the NAc.

Together, these data indicate that the neurochemical and functional changes induced by prefrontal tDCS contribute directly to the observed restoration of cognitive and non-cognitive symptoms in the Tg2576 mouse model.

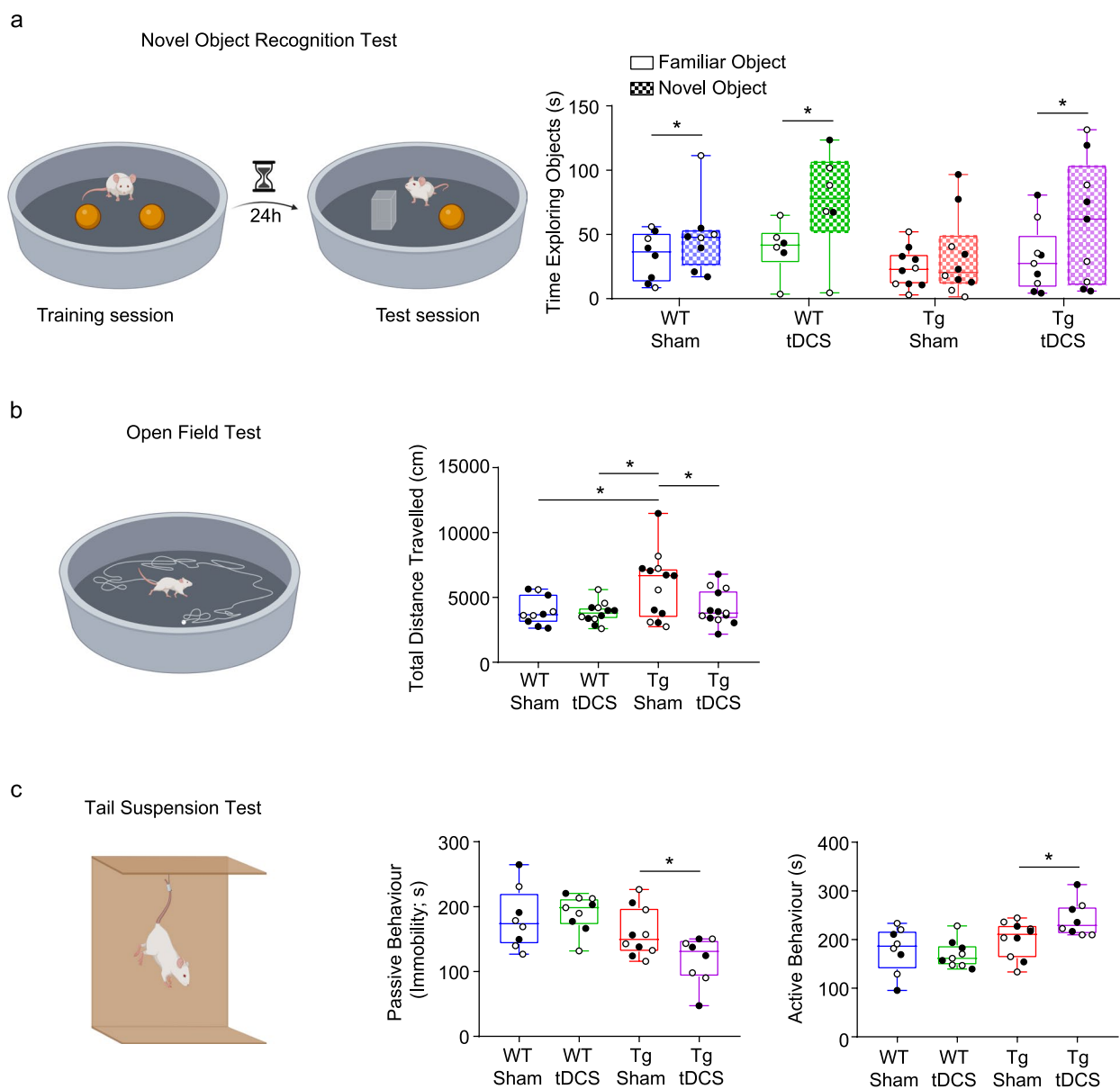


**Fig. 3** Prefrontal tDCS restores cognitive and non-cognitive functions in 7-month-old Tg2576 mice. **a** The graph shows the total time spent exploring objects (novel and/or familiar) during the NOR test, conducted 24 h after the training phase, by 7-month-old WT and Tg2576 mice receiving tDCS or Sham stimulation (WT Sham:  $n = 8$ ; WT tDCS:  $n = 6$ ; Tg Sham:  $n = 10$ ; Tg tDCS:  $n = 9$ ; WT Sham  $*p = 0.0391$  with Wilcoxon matched-pairs test; WT tDCS  $*p = 0.0285$ , Tg tDCS  $*p = 0.0425$  both with Paired  $t$ -test). **b** The plot represents the total locomotor activity, quantified as the distance travelled during the exploration of a novel environment in the open field test, by 7-month-old WT and Tg2576 mice following Sham or tDCS treatment (WT Sham:  $n = 10$ ; WT tDCS:  $n = 12$ ; Tg Sham:  $n = 13$ ; Tg tDCS:  $n = 13$ ; WT Sham–Tg Sham  $*p = 0.0246$ ; WT tDCS–Tg Sham  $*p = 0.0129$ ; Tg Sham–Tg tDCS  $*p = 0.0444$ , all with 2-tailed Welch’s  $t$ -test). **c** The two box-and-whisker plots show antidepressant-like responses in the TST, quantified by the time spent in passive (immobility, *left*) and active (*right*) behaviours, reflecting coping strategies in 7-month-old WT Sham ( $n = 8$ ), WT tDCS ( $n = 9$ ), Tg Sham ( $n = 10$ ) and Tg tDCS ( $n = 8$ ) mice (2-way ANOVA: interaction  $F_{1,31} = 3.968$ ,  $p = 0.0552$ . Tg Sham–Tg tDCS  $*p = 0.0303$  unpaired  $t$ -test, for both active and passive behaviours). [Figure created using BioRender.com]

**Prefrontal tDCS ameliorates neuroinflammation and A $\beta$  plaque accumulation in Tg2576 mice**

Dopaminergic receptors are expressed by different glia cells and their DA-mediated activation was demonstrated to inhibit reactive neuroimmune states and the release of

pro-inflammatory cytokines [43]. Given the importance of DA in blunting neuroinflammation, we next investigated whether prefrontal tDCS, by activating DA neurons in the VTA and restoring DA levels in the hippocampus, could reduce neuroinflammatory responses in Tg2576

mice at both pre-plaque stage (7 months of age) and at an age marked by A $\beta$  plaque accumulation (12 months of age).

7-month-old Tg Sham mice showed an increased number of hippocampal Iba1<sup>+</sup> microglial cells compared to WT mice, with markedly altered morphology as demonstrated by increased somatic area and higher complexity of dendritic branching, typical of reactive microglia. The prefrontal tDCS protocol determined a significant decrease in the number of Iba1<sup>+</sup> cells in Tg tDCS mice (Fig. 4a,b) and, at the same time, changes in morphology toward a less reactive phenotype (Fig. 4c,d; Fig. S3a). Even at 12 months of age, tDCS effectively reduced hippocampal microglia-mediated neuroinflammation in Tg2576 mice. Indeed, stereological cell count revealed a significant reduction of Iba1<sup>+</sup> cell number in Tg tDCS mice compared to all other experimental groups (Fig. 4e,f). Additionally, prefrontal tDCS application in Tg mice was effective in reducing both microglial somatic area and branching complexity (Fig. 4g,h; Fig. S3b), indicating a suppression of microglial response even at an advanced disease stage.

Finally, we investigated the impact of prefrontal tDCS on A $\beta$  load. Analysis of intracellular A $\beta$  levels at 7 months of age showed no differences in Tg tDCS mice compared to Tg Sham mice (Fig. 5a). Yet, Tg tDCS mice at 12 months showed a significant reduction in the number of hippocampal A $\beta$  plaques compared to Tg Sham mice, while plaque size remained unchanged (Fig. 5b).

This suggests that prefrontal tDCS can be a promising tool for reducing A $\beta$  plaque deposition.

## Discussion

This study significantly advances the understanding of prefrontal tDCS as a tool for deep modulation of subcortical brain regions, particularly the dopaminergic VTA, with potential applications in AD therapy. Our results highlight the efficacy of prefrontal tDCS in enhancing dopaminergic neurotransmission in the Tg2576 mouse model of AD, by selectively activating VTA TH<sup>+</sup> neurons. In fact, prefrontal tDCS did not activate TH<sup>+</sup> neurons in the LC, indicating a targeted effect on VTA DA neurons. The observed activation leads to a consequent increase in hippocampal DA outflow, an upregulation of DAT expression in the NAc and improvement of pathophysiological markers and AD-like symptoms.

Prefrontal tDCS studies in different transgenic mouse models of AD generally show improvements in synaptic plasticity, spatial learning, object recognition memory and AD hallmarks like A $\beta$ <sub>1-42</sub> levels and neuroinflammation [91–93]. Our work further adds to these findings in that it offers a potential explanation for the observed improvements, by demonstrating the engagement of the mesocorticolimbic circuit and the potentiation of the DA signalling. Indeed, considering the early and progressive VTA dopaminergic neuronal loss of the Tg2576 model, our results underscore the capability of prefrontal tDCS to effectively circumvent extensive neurodegenerative

(See figure on next page.)

**Fig. 4** Prefrontal tDCS mitigates hippocampal microglia-mediated neuroinflammation in 7- and 12-month-old Tg2576 mice. **a** Confocal images (scale: 50  $\mu$ m) of Iba1<sup>+</sup> cells in the hippocampus of 7-month-old WT and Tg2576 mice receiving tDCS or Sham stimulation. Nuclei are counterstained with DAPI. **b** Stereological count of Iba1<sup>+</sup> cells (WT Sham:  $n = 7$ ; WT tDCS:  $n = 5$ ; Tg Sham:  $n = 4$ ; Tg tDCS:  $n = 4$ ; 2-way RM-ANOVA: interaction,  $F_{1,16} = 6.166$ ,  $p = 0.0245$ ; treatment,  $F_{1,16} = 9.375$ ,  $p = 0.0075$ ; genotype,  $F_{1,16} = 4.763$ ,  $p = 0.0443$ . WT Sham–Tg Sham  $*p = 0.0167$ ; WT tDCS–Tg Sham  $*p = 0.0118$ ; Tg Sham–Tg tDCS  $*p = 0.0116$ , with Tukey's post hoc). **c** Somatic area of microglia (n = 4 mice/group, 2 males and 2 females; 2-way RM-ANOVA: interaction,  $F_{1,12} = 9.344$ ,  $p = 0.0100$ ; treatment,  $F_{1,12} = 2.947$ ,  $p = 0.1117$ ; genotype,  $F_{1,12} = 12.86$ ,  $p = 0.0037$ ; WT Sham–Tg Sham  $**p = 0.0025$ , WT tDCS–Tg Sham  $*p = 0.0128$ , Tg Sham–Tg tDCS  $*p = 0.0246$ , with Tukey's post hoc). **d** 3D-reconstruction of microglia (scale: 10  $\mu$ m) and Sholl analysis (changes are marked by \* for WT Sham vs. Tg Sham and by ° for Tg Sham vs. Tg tDCS; n = 4 mice/group, 2 males and 2 females; 2-way RM-ANOVA: Intersection (genotype): interaction,  $F_{6,36} = 9.002$ ,  $p < 0.0001$ ; distance,  $F_{6,36} = 396.2$ ,  $p < 0.0001$ ; genotype,  $F_{1,6} = 12.18$ ,  $p = 0.0130$ ; WT Sham–Tg Sham  $****p < 0.0001$  at 10–20  $\mu$ m,  $*p = 0.0152$  at 30  $\mu$ m; Intersection (treatment): interaction,  $F_{6,36} = 2.129$ ,  $p = 0.0737$ ; distance,  $F_{6,36} = 295.0$ ,  $p < 0.0001$ ; treatment,  $F_{1,6} = 2.752$ ,  $p = 0.1482$ ; Tg Sham–Tg tDCS: ° $p = 0.0140$  at 20  $\mu$ m; Process length (genotype): interaction,  $F_{6,36} = 14.33$ ,  $p < 0.0001$ ; distance,  $F_{6,36} = 599.5$ ,  $p < 0.0001$ ; genotype,  $F_{1,6} = 13.18$ ,  $p = 0.0110$ ; WT Sham–Tg Sham  $****p < 0.0001$  at 20–30  $\mu$ m; Process length (treatment): interaction,  $F_{6,36} = 3.057$ ,  $p = 0.0160$ ; distance,  $F_{6,36} = 314.0$ ,  $p < 0.0001$ ; treatment,  $F_{1,6} = 3.523$ ,  $p = 0.1096$ ; Tg Sham–Tg tDCS ° $p = 0.0085$  at 20  $\mu$ m, ° $p = 0.0349$  at 30  $\mu$ m, with Sidak's). **e–f** Iba1 staining (scale: 50  $\mu$ m) and plot showing microglia number in 12-month-old WT and Tg2576 mice (WT Sham/WT tDCS/Tg Sham:  $n = 5$  mice/group; Tg tDCS:  $n = 4$  mice; 2-way RM-ANOVA: interaction,  $F_{1,15} = 9.072$ ,  $p = 0.0088$ ; treatment,  $F_{1,15} = 13.51$ ,  $p = 0.0023$ ; genotype,  $F_{1,15} = 7.581$ ,  $p = 0.0148$ ; WT Sham–Tg tDCS  $**p = 0.0025$ , Tg Sham–Tg tDCS  $**p = 0.0018$ , WT tDCS–Tg tDCS  $**p = 0.0061$ ). **g** Somatic area of microglia (n = 4 mice/group, 2 males and 2 females; 2-way RM-ANOVA: interaction,  $F_{1,12} = 4.654$ ,  $p = 0.0520$ ; treatment,  $F_{1,12} = 10.45$ ,  $p = 0.0072$ ; genotype,  $F_{1,12} = 11.10$ ,  $p = 0.0060$ ; WT Sham–Tg Sham  $*p = 0.0102$ , WT tDCS–Tg Sham  $**p = 0.0028$ , Tg Sham–Tg tDCS  $*p = 0.0115$ ). **h** 3D microglia reconstruction and Sholl analysis (n = 4 mice/group, 2 males and 2 females; 2-way RM-ANOVA: Intersection (genotype): interaction,  $F_{6,36} = 2.414$ ,  $p = 0.0460$ ; distance,  $F_{6,36} = 281.1$ ,  $p < 0.0001$ ; genotype,  $F_{1,6} = 0.5911$ ,  $p = 0.4712$ ; WT Sham–Tg Sham  $**p = 0.0065$  at 10  $\mu$ m; Intersection (treatment): interaction,  $F_{6,36} = 5.130$ ,  $p = 0.0007$ ; distance,  $F_{6,36} = 436.1$ ,  $p < 0.0001$ ; treatment,  $F_{1,6} = 23.63$ ,  $p = 0.0028$ ; Tg Sham–Tg tDCS  $****p < 0.0001$  at 10  $\mu$ m, ° $p = 0.0051$  at 20  $\mu$ m. Process length (genotype): interaction,  $F_{6,36} = 3.616$ ,  $p = 0.0066$ ; distance,  $F_{6,36} = 397.1$ ,  $p < 0.0001$ ; genotype,  $F_{1,6} = 0.4088$ ,  $p = 0.5462$ ; WT Sham–Tg Sham  $*p = 0.0123$  at 20  $\mu$ m; Process length (treatment): interaction,  $F_{6,36} = 6.156$ ,  $p = 0.0002$ ; distance,  $F_{6,36} = 682.4$ ,  $p < 0.0001$ ; genotype,  $F_{1,6} = 12.90$ ,  $p = 0.0115$ ; Tg Sham–Tg tDCS ° $p = 0.0426$  at 10  $\mu$ m, ° $p < 0.0001$  at 20  $\mu$ m, with Sidak's)

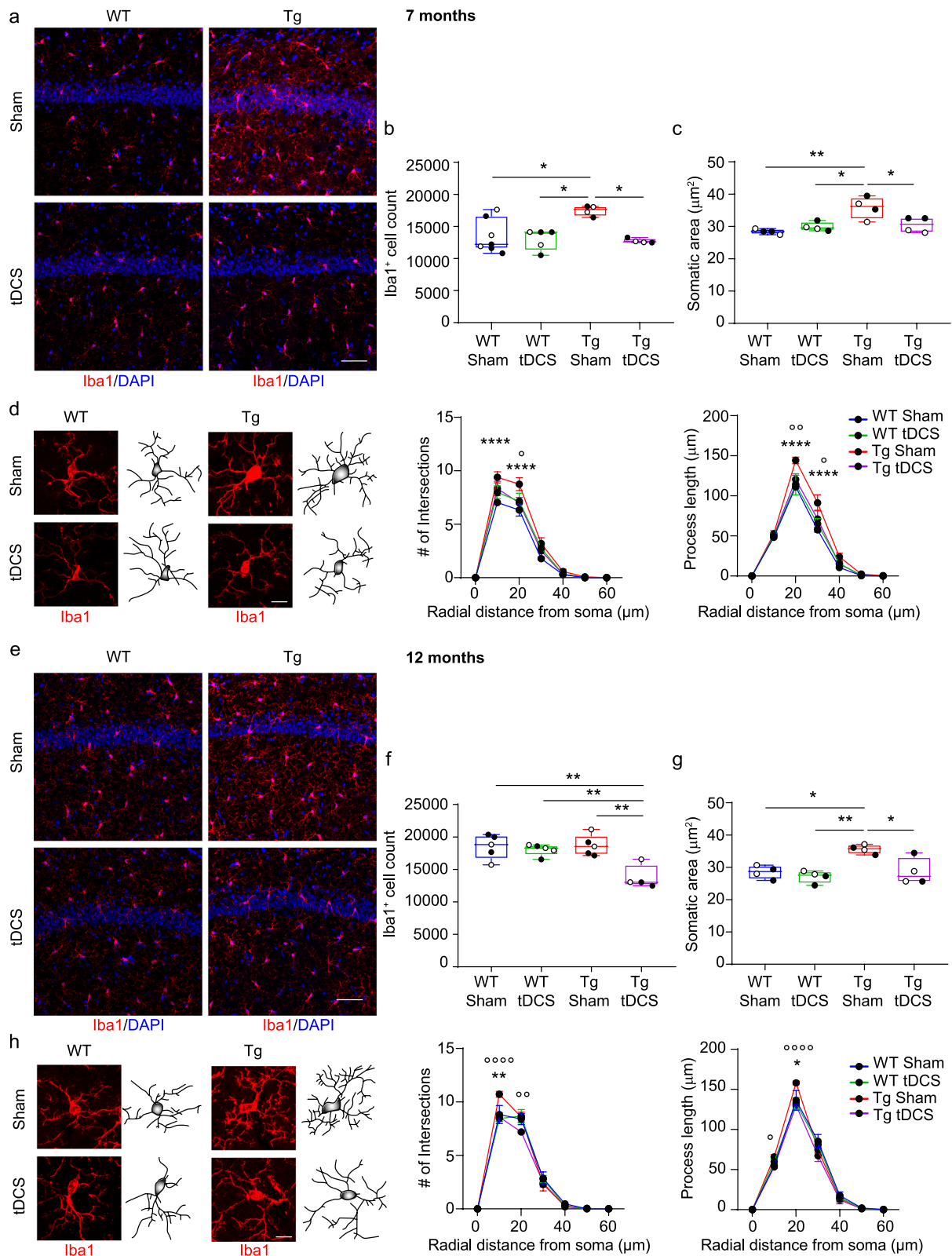


**Fig. 4** (See legend on previous page.)

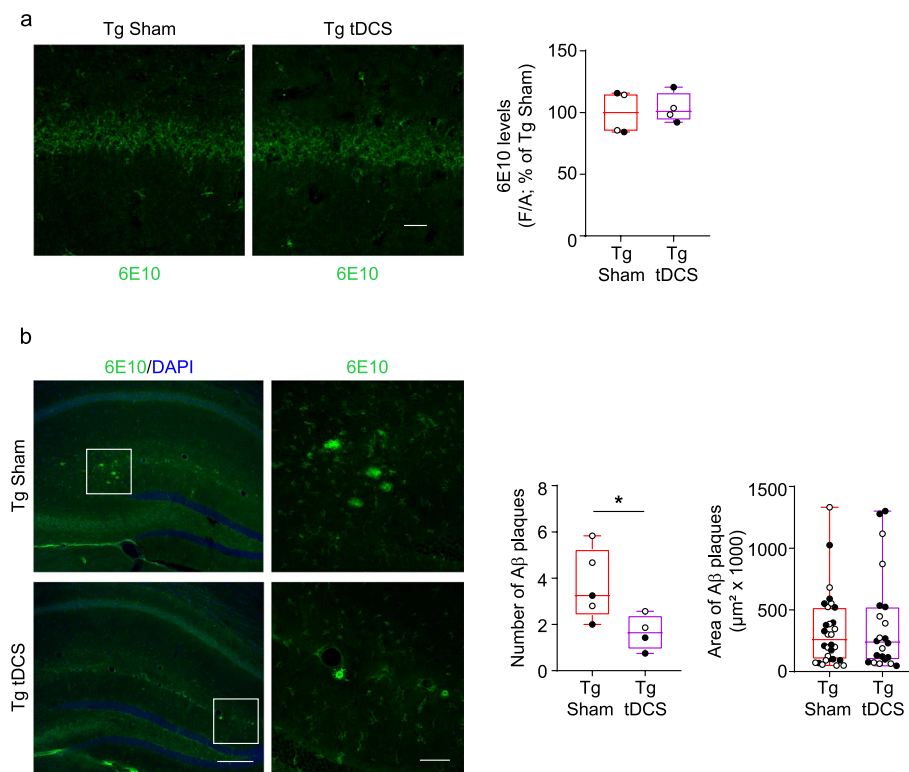


**Fig. 5** Prefrontal tDCS reduces A $\beta$  plaque burden in 12-month-old Tg2576 mice. **a** Representative confocal images showing intracellular A $\beta$  levels (6E10, green) in the hippocampal CA1 region of 7-month-old Tg Sham and Tg tDCS mice (scale bar: 50  $\mu$ m). Plot displays intracellular A $\beta$  levels, measured as mean fluorescence intensity for 6E10 ( $n = 4$  mice/group). **b** Representative confocal images of extracellular A $\beta$  plaques (6E10, green) in the hippocampus of 12-month-old Tg2576 mice receiving Sham or tDCS stimulation (scale bar: 200  $\mu$ m). Nuclei are counterstained with DAPI. The insets (scale bar: 50  $\mu$ m) show individual plaques. The plots on the right report the number of A $\beta$  plaque (left) and plaque area (right) (Plaque number: Tg Sham:  $n = 5$  mice; Tg tDCS:  $n = 4$  mice; \* $p = 0.0453$  unpaired  $t$ -test; Plaque area: Tg Sham:  $n = 30$  plaques/5 mice; Tg tDCS:  $n = 22$  plaques/4 mice)

barriers, driving the activation of the remaining neurons. This observation raises pertinent mechanistic questions regarding the ability of cortical stimulation to recruit dopaminergic activity within pathologically compromised regions. However, it is important to clarify that the stimulation does not necessarily prevent neurodegeneration nor reverse neuronal loss, but likely leverages intact afferent projections from the PFC to the midbrain. Indeed, the PFC significantly influences the VTA and NAc through extensive projections, with PFC terminals synapsing on DA and non-DA neurons in the VTA and affecting DA release in the hippocampus and NAc. Functional coupling between the PFC and VTA indicates a dynamic exchange of excitatory and inhibitory inputs [94–96]. Our study suggests that prefrontal tDCS enhances excitatory input to the DA neurons of the VTA, resulting in increased dopaminergic output to the hippocampus and NAc, in line with the multiple studies attributing the effects of prefrontal tDCS to the engagement of the mesocorticolimbic circuit and the enhancement of DA availability in both animal models and

humans [58, 60, 61, 63, 64, 66, 69]. Furthermore, anatomical studies reveal that projections from the PFC innervate the entire midbrain, including both the VTA and the Substantia Nigra *pars compacta* (SNpc), albeit with a relatively sparse distribution [97]. This cortical innervation suggests that tDCS applied over the PFC potentially engages not only surviving VTA neurons, but also dopaminergic populations within the SNpc, which are not affected by neurodegeneration in the Tg2576 model [16]. While the SNpc is traditionally linked to motor function via its projections to the dorsal striatum, it also provides dopaminergic afferents to limbic structures, including the hippocampus [98]. Thus, the observed behavioural and neurochemical effects may not be exclusively VTA-dependent but rather indicative of a broader, coordinated activation of the entire midbrain dopaminergic system.

Our findings also align with previous evidence demonstrating that prefrontal tDCS can enhance dopaminergic signalling even in the context of Parkinson's Disease (PD). Indeed, in an MPTP mouse model, tDCS prevents the loss of TH<sup>+</sup> neurons in the SNpc, thereby preserving

dopaminergic content in the striatum [64]. Collectively, these results highlight a dual therapeutic potential of prefrontal tDCS: neuroprotection in earlier stages and functional modulation in advanced neurodegeneration. This raises the question of whether early tDCS application in the Tg2576 model could have similar neuroprotective effects as seen in the PD mouse model.

In the hippocampus, basal DA levels remained unchanged following prefrontal tDCS. Nonetheless, a significant increase in DA release was observed in Tg2576 mice post-KCl-induced depolarization, indicating dopaminergic terminals became more responsive to stimulation. Mechanistically, this suggests that tDCS exerts a priming effect, augmenting presynaptic excitability and calcium influx, which collectively facilitates vesicular DA release. Repeated depolarization events, such as those induced by tDCS, may lower the threshold for activity-dependent release or promote synaptic vesicle mobilization, resulting in a more readily releasable DA pool. A similar mechanism may be involved in the facilitation of LTP observed in our electrophysiological experiments, where Tg tDCS mice exhibited a marked enhancement of synaptic plasticity in CA3-CA1 synapses. In both paradigms—KCl perfusion during microdialysis and HFS in electrophysiology experiments—the system appears to respond with a potentiated dopaminergic output, which is crucial for gating long-term synaptic adaptations. This mechanism aligns with well-established models of dopaminergic modulation of hippocampal plasticity, where D1-like receptor activation in CA1 pyramidal neurons promotes intracellular signalling cascades essential for the induction and maintenance of LTP and memory consolidation [99, 100]. While our study did not directly investigate the long-term consequences of enhanced DA release, extensive evidence support the role of dopaminergic facilitation of LTP in strengthening memory traces, particularly in novelty and emotionally tagged learning. Given that DA signalling is typically impaired in AD context [16, 17], pharmacological treatments targeting D1/D5 receptors have been shown to rescue hippocampal plasticity and cognitive function [16, 17, 26–34]. Therefore, the capacity of tDCS to enhance the DA neuron responsiveness may have important implications for re-establishing the permissive neurochemical environment required for plasticity and learning. The improvements in synaptic function and cognitive performance observed in tDCS-treated Tg2576 mice likely reflect a direct re-engagement of mesocorticolimbic dopaminergic circuits in response to salient input. In addition to the mechanisms proposed here, previous studies [52, 54, 101, 102] have identified other pathways through which tDCS may facilitate synaptic plasticity, including modulation of NMDA receptor activity, promotion of BDNF

expression and rebalancing of excitatory/inhibitory neurotransmission. These complementary mechanisms may also contribute to creating a neurochemical environment conducive to plasticity.

Several lines of evidence suggest that tDCS enhances cognitive functions in both healthy populations and animal models without neuropathology. However, in AD, clinical studies have shown mixed results, highlighting the need for robust preclinical research to refine and optimize tDCS protocols [103]. Our study, the first to investigate prefrontal tDCS in the Tg2576 model, reveals the potential of this non-invasive treatment in restoring object recognition memory, normalizing locomotion and reducing depressive-like behaviours. This indicates that the neuromodulatory effects of prefrontal tDCS extend beyond cognitive enhancement, modulating non-cognitive behaviours such as locomotion and affective responses. Specifically, prefrontal tDCS normalized the hyperlocomotion observed in Tg2576 mice in the open field test, highlighting its capacity to regulate activity levels through the modulation of mesolimbic circuitry, in line with the established role of the VTA in motivated behaviour. The involvement of the VTA in locomotor control is further supported by studies on the medial NAc inputs to the VTA, where optogenetic stimulation of medial NAc terminals induces a sustained post-stimulation reduction in general locomotor activity. This suggests that reciprocal interactions between the medial NAc and the VTA dynamically shape locomotor behaviour through mechanisms linked to motivational states and post-stimulation adaptations [104]. Similarly, Tg tDCS mice exhibited reduced immobility and increased active behaviours in the TST, indicating antidepressant-like effects and an enhanced motivational drive, aligning with the central role of DA in these processes [105, 106]. These observations support the notion of a presynaptic priming mechanism wherein tDCS lowers the threshold for dopaminergic activation, preferentially engaging DA neurons projecting to the NAc. This enhanced DA release in the NAc likely amplifies motivational drive, facilitating behavioural engagement. Notably, this interpretation is reinforced by the observed upregulation of DAT levels in both NAc core and shell—areas crucial for goal-directed behaviours, reward processing and affective regulation. Collectively, our findings suggest that the recovery of the midbrain dopaminergic signalling via prefrontal tDCS extends its functional impact across its downstream targets, integrating motivational, cognitive and affective processes.

Importantly, prefrontal tDCS could mitigate neuroinflammation in Tg2576 hippocampi. Neuroinflammation is a key feature of early AD that worsens disease progression and symptom severity, and the fact that prefrontal

tDCS treatment in Tg2576 mice reduces microglial reactivity further emphasizes its therapeutic potential. This is in line with existing literature showing that tDCS modulates neuroinflammation by reducing pro-inflammatory cytokine release and glial cell activation [56, 57, 107]. Although not directly proven, the ability of prefrontal tDCS to ameliorate microglia-mediated neuroinflammation in Tg2576 mice could result from increased hippocampal DA outflow, given the well-established anti-inflammatory role of DA [42–45].

Despite decades of research, effective disease-modifying therapies remain limited. Recent advancements have emerged with the development of monoclonal antibodies targeting A $\beta$  [108, 109]. While these treatments represent important progress in the field, their effectiveness is limited to early disease stages, and they require regular intravenous administration and careful monitoring through Magnetic Resonance Imaging scans [110]. Additional challenges, such as patient ineligibility, lack of clinically relevant improvements after therapy, high costs and significant side effects, underscore the ongoing limitations in AD therapeutics. These include the need for early intervention, broader patient inclusion, less invasive treatment options and a therapeutic approach that targets multiple pathological mechanisms beyond A $\beta$  accumulation [111–114]. These limitations underscore the need for complementary therapeutic approaches that could address broader aspects of AD pathophysiology. In this framework, prefrontal tDCS offers a non-invasive alternative: beyond the ability to activate the mesocorticolimbic system and attenuate the neuroinflammatory response, prefrontal tDCS is effective in reducing A $\beta$  burden in Tg2576 mice. Intriguingly, tDCS might reduce A $\beta$  plaques either by promoting a pro-phagocytic microglia response or by enhancing DA tone, given the emerging role of DA in facilitating enzymatic clearance and disaggregation of extracellular amyloid deposits [46, 48]. Nonetheless, further investigation is warranted to delineate the temporal dynamics and molecular mediators involved in these processes.

Additionally, prefrontal tDCS can be a valid alternative to Deep Brain Stimulation (DBS) and Transcranial Magnetic Stimulation (TMS) for AD treatment. While DBS is highly effective, it is invasive and costly. TMS, though non-invasive, can be uncomfortable due to high-intensity pulses and is operative-dependent, limiting its home-based application. Instead, tDCS, with its low-intensity currents, is painless, cost-effective and portable, allowing for continuous stimulation and broader clinical applications, including the possibility of safe home-based treatment protocols. By using a stimulation protocol without anaesthesia in Tg2576 mice, our study enhances the physiological relevance of the findings, ensuring that the

neural and behavioural responses accurately reflect the effects of tDCS.

### Limitations

Despite the promising results of our study, limitations must be acknowledged. The Tg2576 model represents a specific aspect of AD pathology and it does not fully recapitulate the complexity of human AD. The extent to which our findings translate to clinical populations remains uncertain, necessitating further validation in additional preclinical models and, ultimately, in human trials. Moving toward human translation, it will be critical to refine stimulation protocols to align with the clinical parameters—particularly optimizing current density delivered and electrode configuration—while adhering within established safety guidelines. Future research should prioritize this translational approach to systematically evaluate the efficacy and tolerability of prefrontal tDCS in MCI and AD patients. Furthermore, the development of precisely calibrated and individualized protocols will be essential to facilitate its integration into clinical practice, ensuring both therapeutic efficacy and patient safety. Another noteworthy aspect is our focus on short-term outcomes following tDCS treatment. The long-term sustainability of its effects, as well as potential compensatory mechanisms that may arise over time, remain unexplored. This keeps open the possibility of future longitudinal assessments to determine the persistence of tDCS-induced benefits and potential long-term safety concerns. These limitations notwithstanding, our findings provide a strong foundation for further research into tDCS as a non-invasive neuromodulatory intervention for AD, supporting its potential integration into multimodal treatment strategies.

### Conclusions

Despite these limitations, our study provides compelling evidence for the therapeutic potential of prefrontal tDCS in AD, highlighting its effects on dopaminergic modulation, synaptic plasticity and behaviour, as well as its role in reducing neuroinflammation and amyloid pathology. These findings lay the groundwork for future research and clinical applications, with the potential to transform the landscape of non-invasive treatments for neurodegenerative disorders.

### Abbreviations

A $\beta$	Amyloid- $\beta$
aCSF	Artificial cerebrospinal fluid
AD	Alzheimer's Disease
DA	Dopamine
DAT	Dopamine transporter
DBS	Deep Brain Stimulation
fEPSP	field Excitatory postsynaptic potential
LC	Locus Coeruleus
LTP	Long-Term Potentiation

MCI	Mild Cognitive Impairment
NAC	Nucleus Accumbens
NE	Norepinephrine
NOR	Novel Object Recognition
NPS	Neuropsychiatric symptoms
PB	Phosphate Buffer
PD	Parkinson's Disease
PFC	Prefrontal Cortex
SNpc	Substantia Nigra pars compacta
tDCS	Transcranial Direct Current Stimulation
TH	Tyrosine Hydroxylase
TMS	Transcranial Magnetic Stimulation
TST	Tail Suspension Test
UPLC	Ultra-Performance Liquid Chromatography
VTA	Ventral Tegmental Area
WT	Wild-Type

## Supplementary Information

The online version contains supplementary material available at <https://doi.org/10.1186/s13195-025-01736-4>.

Additional file 1: Supplemental Figures and legends; Supplemental Table. Figure S1: Training phase in the NOR test; Figure S2: Prefrontal tDCS restores DAT levels in the NAC of 7-month-old Tg2576 mice; Figure S3: Analysis of additional morphometric variables in microglia cells of 7- and 12-month-old WT and Tg2576 mice; Table S1: Power analysis output values.

## Acknowledgements

We thank Dr Wirz for assistance with animal caring.

## Authors' contributions

E.C.L., P.K. and M.D.A. conceived the study; M.L.D.P., E.C.L., S.P.A., R.C., M.D.S. and L.B. designed and performed surgical procedures, tDCS, microdialysis and behavioural experiments; G.L., L.L.B., A.N. and E.C. designed and performed immunofluorescence experiments, stereology and Sholl Analysis; M.L.D.P. and P.K. carried out the electrophysiological experiments; M.L.D.P., P.K., L.L.B., E.C.L. and M.D.A. wrote the manuscript; all authors discussed results, commented on the manuscript, read and approved the final version.

## Funding

L.L.B. was supported by an under-40 grant from the Italian Association for Alzheimer's Research [AIRALZH-AGYR2021] and by the Strategic University Projects – Young Researcher Independence [YRG2021] from the Università Campus Bio-Medico di Roma (Rome, Italy). P.K. was supported by the Italian Ministry of Health [Research Grant: GR-2019–12370446] and by the American Alzheimer's Association [AARG-22–922961]. E.C.L. was supported by the Italian Ministry of Health [Research Grant: GR-2018–12365991]. M.D.A. was supported by the American Alzheimer's Association [AARG-18–566270; AARG-21–851219], by the Italian Ministry of Health [Research Grant: RF-2018–12365527], by the Italian Ministry of Universities and Research [Prot. 2020Z73J5A] and by Fondazione Roma (Rome, Italy).

## Data availability

The datasets supporting the findings of this study are included within the article and the supplementary materials. Raw data can also be freely available by the corresponding authors upon request.

## Declarations

### Ethics approval and consent to participate

All animal procedures were conducted in accordance with the ARRIVE procedures and the ethical guidelines of the European Council Directive (2010/63/EU). Experimental approval was obtained from the Italian Ministry of Health (protocol #501-2019PPR).

### Consent for publication

Not applicable.

## Competing interests

The authors declare no competing interests.

## Author details

<sup>1</sup>Department of Medicine and Surgery, Università Campus Bio-Medico Di Roma, Via Alvaro del Portillo, 21, 00128 Rome, Italy. <sup>2</sup>Department of Sciences and Technologies for Sustainable Development and One Health, Università Campus Bio-Medico Di Roma, Via Alvaro del Portillo, 21, 00128 Rome, Italy. <sup>3</sup>Department of Experimental Neurosciences, IRCCS Santa Lucia Foundation, Via del Fosso Di Fiorano, 64, 00143 Rome, Italy. <sup>4</sup>Department of Psychology, Sapienza University of Rome, P.Le Aldo Moro, 5, 00185 Rome, Italy. <sup>5</sup>Child Psychopathology Unit, IRCCS Eugenio Medea, Via Don Luigi Monza, 20, 23842 Bosisio Parini, Italy. <sup>6</sup>National Research Council (CNR), Institute for Complex System (ISC), Via Dei Taurini, 19, 00185 Rome, Italy. <sup>7</sup>Istituto Di Ricovero E Cura a Carattere Scientifico (IRCCS) Neuromed, Via Atinense, 18, 86077 Pozzilli, Italy. <sup>8</sup>Department of Psychology, International Telematic University Uninet-tuno, Corso Vittorio Emanuele II, 39, 00186 Rome, Italy.

Received: 17 February 2025 Accepted: 7 April 2025

Published online: 29 April 2025

## References

- Jack CR, Andrews SJ, Beach TG, Buracchio T, Dunn B, Graf A, et al. Revised criteria for the diagnosis and staging of Alzheimer's disease. *Nat Med*. 2024;30:2121–4.
- Lloret A, Esteve D, Lloret M-A, Cervera-Ferri A, Lopez B, Nepomuceno M, et al. When Does Alzheimer's Disease Really Start? The Role of Biomarkers. *Int J Mol Sci*. 2019;20:5536.
- Zhang J, Zhang Y, Wang J, Xia Y, Zhang J, Chen L. Recent advances in Alzheimer's disease: mechanisms, clinical trials and new drug development strategies. *Sig Transduct Target Ther*. 2024;9:1–35.
- Skandalakis GP, Neudorfer C, Payne CA, Bond E, Tavakkoli AD, Barrios-Martinez J, et al. Establishing connectivity through microdissections of midbrain stimulation-related neural circuits. *Brain*. 2024;147:3083–98.
- Iaccarino L, Sala A, Caminiti SP, Presotto L, Perani D. Alzheimer's Disease Neuroimaging Initiative In vivo MRI Structural and PET Metabolic Connectivity Study of Dopamine Pathways in Alzheimer's Disease. *J Alzheimers Dis*. 2020;75:1003–16.
- Manca R, De Marco M, Soininen H, Ruffini L, Venneri A. Changes in neurotransmitter-related functional connectivity along the Alzheimer's disease continuum. *Brain Commun*. 2025;7(1):fcf008. <https://doi.org/10.1093/braincomms/fcaf008>.
- Manca R, Valera-Bermejo JM, Venneri A, Alzheimer's Disease Neuroimaging Initiative. Accelerated atrophy in dopaminergic targets and medial temporo-parietal regions precedes the onset of delusions in patients with Alzheimer's disease. *Eur Arch Psychiatry Clin Neurosci*. 2023;273:229–41.
- Sala A, Caminiti SP, Presotto L, Pilotto A, Liguori C, Chiaravalloti A, et al. In vivo human molecular neuroimaging of dopaminergic vulnerability along the Alzheimer's disease phases. *Alzheimers Res Ther*. 2021;13:187.
- Serra L, D'Amelio M, Esposito S, Di Domenico C, Koch G, Marra C, et al. Ventral Tegmental Area Disconnection Contributes Two Years Early to Correctly Classify Patients Converted to Alzheimer's Disease: Implications for Treatment. *J Alzheimers Dis*. 2021;82:985–1000.
- Serra L, D'Amelio M, Di Domenico C, Dipasquale O, Marra C, Mercuri NB, et al. In vivo mapping of brainstem nuclei functional connectivity disruption in Alzheimer's disease. *Neurobiol Aging*. 2018;72:72–82.
- Venneri A, De Marco M. Reduced monoaminergic nuclei MRI signal detectable in pre-symptomatic older adults with future memory decline. *Sci Rep*. 2020;10:18707.
- Zhang Y, Liang Y, Gu Y. The dopaminergic system and Alzheimer's disease. *Neural Regen Res*. 2025;20:2495–512.
- De Marco M, Venneri A. Volume and connectivity of the Ventral Tegmental Area are linked to neurocognitive signatures of Alzheimer's disease in Humans. *J Alzheimers Dis*. 2018;63:167–80.
- Pilotto A, Galli A, Sala A, Caminiti SP, Presotto L, Liguori C, et al. Dopaminergic deficits along the spectrum of Alzheimer's disease. *Mol Psychiatry* [Internet]. 2025 [cited 2025 Feb 7]; Available from: <https://www.nature.com/articles/s41380-025-02913-5>

15. Krashia P, Spoletti E, D'Amelio M. The VTA dopaminergic system as diagnostic and therapeutic target for Alzheimer's disease. *Front Psychiatry*. 2022;13:1039725.
16. Nobili A, Latagliata EC, Viscomi MT, Cavallucci V, Cutuli D, Giacobazzo G, et al. Dopamine neuronal loss contributes to memory and reward dysfunction in a model of Alzheimer's disease. *Nat Commun*. 2017;8:14727.
17. Cordella A, Krashia P, Nobili A, Pignataro A, La Barbera L, Viscomi MT, et al. Dopamine loss alters the hippocampus-nucleus accumbens synaptic transmission in the Tg2576 mouse model of Alzheimer's disease. *Neurobiol Dis*. 2018;116:142–54.
18. La Barbera L, Nobili A, Cauzzi E, Paoletti I, Federici M, Saba L, et al. Upregulation of Ca<sup>2+</sup>-binding proteins contributes to VTA dopamine neuron survival in the early phases of Alzheimer's disease in Tg2576 mice. *Mol Neurodegener*. 2022;17:76.
19. La Barbera L, Vedele F, Nobili A, Krashia P, Spoletti E, Latagliata EC, et al. Nilotinib restores memory function by preventing dopaminergic neuron degeneration in a mouse model of Alzheimer's Disease. *Prog Neurobiol*. 2021;202: 102031.
20. Spoletti E, La Barbera L, Cauzzi E, De Paolis ML, Saba L, Marino R, et al. Dopamine neuron degeneration in the Ventral Tegmental Area causes hippocampal hyperexcitability in experimental Alzheimer's Disease. *Mol Psychiatry*. 2024;29(5):1265–80. <https://doi.org/10.1038/s41380-024-02408-9>.
21. Spoletti E, Krashia P, La Barbera L, Nobili A, Lupascu CA, Giacalone E, et al. Early derailment of firing properties in CA1 pyramidal cells of the ventral hippocampus in an Alzheimer's disease mouse model. *Exp Neurol*. 2021;350:113969.
22. Blankenship HE, Carter KA, Pham KD, Cassidy NT, Markiewicz AN, Thellmann MI, et al. VTA dopamine neurons are hyperexcitable in 3xTg-AD mice due to casein kinase 2-dependent SK channel dysfunction. *Nat Commun*. 2024;15:9673.
23. Gloria Y, Ceyzériat K, Tsartsalis S, Millet P, Tournier BB. Dopaminergic dysfunction in the 3xTg-AD mice model of Alzheimer's disease. *Sci Rep*. 2021;11:19412.
24. Moreno-Castilla P, Rodríguez-Duran LF, Guzman-Ramos K, Barcenas-Femat A, Escobar ML, Bermudez-Rattoni F. Dopaminergic neurotransmission dysfunction induced by amyloid- $\beta$  transforms cortical long-term potentiation into long-term depression and produces memory impairment. *Neurobiol Aging*. 2016;41:187–99.
25. Vorobyov V, Bakharev B, Medvinskaya N, Nesterova I, Samokhin A, Deev A, et al. Loss of midbrain dopamine neurons and altered apomorphine EEG effects in the 5xFAD mouse model of Alzheimer's disease. *J Alzheimers Dis*. 2019;70:241–56.
26. Ambrée O, Richter H, Sachser N, Lewejohann L, Dere E, de Souza Silva MA, et al. Levodopa ameliorates learning and memory deficits in a murine model of Alzheimer's disease. *Neurobiol Aging*. 2009;30:1192–204.
27. Guzmán-Ramos K, Moreno-Castilla P, Castro-Cruz M, McGaugh JL, Martínez-Coria H, LaFerla FM, et al. Restoration of dopamine release deficits during object recognition memory acquisition attenuates cognitive impairment in a triple transgenic mice model of Alzheimer's disease. *Learn Mem*. 2012;19:453–60.
28. Hao J-R, Sun N, Lei L, Li X-Y, Yao B, Sun K, et al. L-Stepholidine rescues memory deficit and synaptic plasticity in models of Alzheimer's disease via activating dopamine D1 receptor/PKA signaling pathway. *Cell Death Dis*. 2015;6:e1965.
29. Himeno E, Ohyagi Y, Ma L, Nakamura N, Miyoshi K, Sakae N, et al. Apomorphine treatment in Alzheimer mice promoting amyloid- $\beta$  degradation. *Ann Neurol*. 2011;69:248–56.
30. Jürgensen S, Antonio LL, Mussi GEA, Brito-Moreira J, Bomfim TR, De Felice FG, et al. Activation of D1/D5 dopamine receptors protects neurons from synapse dysfunction induced by amyloid-beta oligomers. *J Biol Chem*. 2011;286:3270–6.
31. Liu Y, Yoo M-J, Savonenko A, Stirling W, Price DL, Borchelt DR, et al. Amyloid pathology is associated with progressive monoaminergic neurodegeneration in a transgenic mouse model of Alzheimer's disease. *J Neurosci*. 2008;28:13805–14.
32. Pazini AM, Gomes GM, Villarinho JG, da Cunha C, Pinheiro F, Ferreira APO, et al. Selegiline reverses  $\alpha\beta_{25-35}$ -induced cognitive deficit in male mice. *Neurochem Res*. 2013;38:2287–94.
33. Tsunekawa H, Noda Y, Mouri A, Yoneda F, Nabeshima T. Synergistic effects of selegiline and donepezil on cognitive impairment induced by amyloid beta (25–35). *Behav Brain Res*. 2008;190:224–32.
34. Yuan Xiang P, Janc O, Grochowska KM, Kreuz MR, Reymann KG. Dopamine agonists rescue A $\beta$ -induced LTP impairment by Src-family tyrosine kinases. *Neurobiol Aging*. 2016;40:98–102.
35. Koch G, Di Lorenzo F, Bonni S, Giacobbe V, Bozzali M, Caltagirone C, et al. Dopaminergic modulation of cortical plasticity in Alzheimer's disease patients. *Neuropsychopharmacology*. 2014;39:2654–61.
36. Koch G, Esposito Z, Codecà C, Mori F, Kusayanagi H, Monteleone F, et al. Altered dopamine modulation of LTD-like plasticity in Alzheimer's disease patients. *Clin Neurophysiol*. 2011;122:703–7.
37. Martorana A, Koch G. Is dopamine involved in Alzheimer's disease? *Front Aging Neurosci*. 2014;6:252.
38. Monteverde A, Gnemmi P, Rossi F, Monteverde A, Finali GC. Selegiline in the treatment of mild to moderate Alzheimer-type dementia. *Clin Ther*. 1990;12:315–22.
39. Lisman JE, Grace AA. The Hippocampal-VTA Loop: Controlling the Entry of Information into Long-Term Memory. *Neuron*. 2005;46:703–13.
40. Rosen ZB, Cheung S, Siegelbaum SA. Midbrain dopamine neurons bidirectionally regulate CA3-CA1 synaptic drive. *Nat Neurosci*. 2015;18:1763–71.
41. Sayegh FJP, Mouldous L, Macri C, Pi Macedo J, Lejards C, Rampon C, et al. Ventral tegmental area dopamine projections to the hippocampus trigger long-term potentiation and contextual learning. *Nat Commun*. 2024;15:4100.
42. Feng Y, Lu Y. Immunomodulatory Effects of Dopamine in Inflammatory Diseases. *Front Immunol*. 2021;12:663102.
43. Possemato E, La Barbera L, Nobili A, Krashia P, D'Amelio M. The role of dopamine in NLRP3 inflammasome inhibition: Implications for neurodegenerative diseases. *Ageing Res Rev*. 2023;87: 101907.
44. Xia Q-P, Cheng Z-Y, He L. The modulatory role of dopamine receptors in brain neuroinflammation. *Int Immunopharmacol*. 2019;76:105908.
45. Yan Y, Jiang W, Liu L, Wang X, Ding C, Tian Z, et al. Dopamine controls systemic inflammation through inhibition of NLRP3 inflammasome. *Cell*. 2015;160:62–73.
46. Cataldi R, Chia S, Pisani K, Ruggeri FS, Xu CK, Šneideris T, et al. A dopamine metabolite stabilizes neurotoxic amyloid- $\beta$  oligomers. *Commun Biol*. 2021;4:1–10.
47. Di Giovanni S, Eleuteri S, Paleologou KE, Yin G, Zweckstetter M, Carrupt P-A, et al. Entacapone and tolcapone, two catechol O-methyltransferase inhibitors, block fibril formation of alpha-synuclein and beta-amyloid and protect against amyloid-induced toxicity. *J Biol Chem*. 2010;285:14941–54.
48. Li J, Zhu M, Manning-Bog AB, Di Monte DA, Fink AL. Dopamine and L-dopa disaggregate amyloid fibrils: implications for Parkinson's and Alzheimer's disease. *FASEB J*. 2004;18:962–4.
49. Watamura N, Kakiya N, Fujioka R, Kamano N, Takahashi M, Nilsson P, et al. The dopaminergic system promotes neprilysin-mediated degradation of amyloid- $\beta$  in the brain. *Sci Signal*. 2024;17:eadk1822.
50. Nitsche MA, Seeber A, Frommann K, Klein CC, Rochford C, Nitsche MS, et al. Modulating parameters of excitability during and after transcranial direct current stimulation of the human motor cortex. *J Physiol*. 2005;568:291–303.
51. Monte-Silva K, Kuo M-F, Hessenthaler S, Fresnoza S, Liebetanz D, Paulus W, et al. Induction of late LTP-like plasticity in the human motor cortex by repeated non-invasive brain stimulation. *Brain Stimul*. 2013;6:424–32.
52. Fritsch B, Reis J, Martinowich K, Schambra HM, Ji Y, Cohen LG, et al. Direct current stimulation promotes BDNF-dependent synaptic plasticity: potential implications for motor learning. *Neuron*. 2010;66:198–204.
53. Vasu SO, Kaphzan H. Direct Current Stimulation Modulates Synaptic Facilitation via Distinct Presynaptic Calcium Channels. *Int J Mol Sci*. 2023;24:16866.
54. Podda MV, Cocco S, Mastrodonato A, Fusco S, Leone L, Barbati SA, et al. Anodal transcranial direct current stimulation boosts synaptic plasticity and memory in mice via epigenetic regulation of Bdnf expression. *Sci Rep*. 2016;6:22180.
55. Antonenko D, Schubert F, Bohm F, Ittermann B, Aydin S, Hayek D, et al. tDCS-Induced Modulation of GABA Levels and Resting-State Functional Connectivity in Older Adults. *J Neurosci*. 2017;37:4065–73.

56. Guo T, Fang J, Tong ZY, He S, Luo Y. Transcranial Direct Current Stimulation Ameliorates Cognitive Impairment via Modulating Oxidative Stress, Inflammation, and Autophagy in a Rat Model of Vascular Dementia. *Front Neurosci*. 2020;14:28.
57. Callai EMM, Zin LEF, Catarina LS, Ponzo D, Gonçalves CAS, Vizuete AFK, et al. Evaluation of the immediate effects of a single transcranial direct current stimulation session on astrocyte activation, inflammatory response, and pain threshold in naïve rats. *Behav Brain Res*. 2022;428:113880.
58. Bunai T, Hirokawa T, Kikuchi M, Fukai M, Yokokura M, Ito S, et al. tDCS-induced modulation of GABA concentration and dopamine release in the human brain: A combination study of magnetic resonance spectroscopy and positron emission tomography. *Brain Stimul*. 2021;14:154–60.
59. Chib VS, Yun K, Takahashi H, Shimojo S. Noninvasive remote activation of the ventral midbrain by transcranial direct current stimulation of prefrontal cortex. *Transl Psychiatry*. 2013;3: e268.
60. Fonteneau C, Redoute J, Haesebaert F, Le Bars D, Costes N, Suaud-Chagny M-F, et al. Frontal Transcranial Direct Current Stimulation Induces Dopamine Release in the Ventral Striatum in Human. *Cereb Cortex*. 2018;28:2636–46.
61. Fukai M, Bunai T, Hirokawa T, Kikuchi M, Ito S, Minabe Y, et al. Endogenous dopamine release under transcranial direct-current stimulation governs enhanced attention: a study with positron emission tomography. *Transl Psychiatry*. 2019;9:1–10.
62. Imburgio MJ, Ballard HK, Cornwall AC, Worthy DA, Bernard JA, Orr JM. Preliminary effects of prefrontal tDCS on dopamine-mediated behavior and psychophysiology. *Behav Brain Res*. 2021;402:113091.
63. Leffa DT, de Souza A, Scarabelot VL, Medeiros LF, de Oliveira C, Grevet EH, et al. Transcranial direct current stimulation improves short-term memory in an animal model of attention-deficit/hyperactivity disorder. *Eur Neuropsychopharmacol*. 2016;26:368–77.
64. Lu C, Wei Y, Hu R, Wang Y, Li K, Li X. Transcranial Direct Current Stimulation Ameliorates Behavioral Deficits and Reduces Oxidative Stress in 1-Methyl-4-Phenyl-1,2,3,6-Tetrahydropyridine-Induced Mouse Model of Parkinson's Disease. *Neuromodulation: Technology at the Neural Interface*. 2015;18:442–7.
65. Meyer B, Mann C, Götz M, Gerlicher A, Saase V, Yuen KSL, et al. Increased Neural Activity in Mesostriatal Regions after Prefrontal Transcranial Direct Current Stimulation and L-DOPA Administration. *J Neurosci*. 2019;39:5326–35.
66. Peanlikhit T, Van Waes V, Pedron S, Risold P-Y, Haffen E, Etiévant A, et al. The antidepressant-like effect of tDCS in mice: A behavioral and neurobiological characterization. *Brain Stimul*. 2017;10:748–56.
67. Polanía R, Paulus W, Nitsche MA. Modulating cortico-striatal and thalamo-cortical functional connectivity with transcranial direct current stimulation. *Hum Brain Mapp*. 2012;33:2499–508.
68. Takano Y, Yokawa T, Masuda A, Niimi J, Tanaka S, Hironaka N. A rat model for measuring the effectiveness of transcranial direct current stimulation using fMRI. *Neurosci Lett*. 2011;491:40–3.
69. Tanaka T, Takano Y, Tanaka S, Hironaka N, Kobayashi K, Hanakawa T, et al. Transcranial direct-current stimulation increases extracellular dopamine levels in the rat striatum. *Front Syst Neurosci*. 2013;7:6.
70. Weber MJ, Messing SB, Rao H, Detre JA, Thompson-Schill SL. Prefrontal transcranial direct current stimulation alters activation and connectivity in cortical and subcortical reward systems: a tDCS-fMRI study. *Hum Brain Mapp*. 2014;35:3673–86.
71. Hsiao K, Chapman P, Nilsen S, Eckman C, Harigaya Y, Younkin S, et al. Correlative memory deficits, Aβ elevation, and amyloid plaques in transgenic mice. *Science*. 1996;274:99–102.
72. Bikson M, Grossman P, Thomas C, Zannou AL, Jiang J, Adnan T, et al. Safety of Transcranial Direct Current Stimulation: Evidence Based Update 2016. *Brain Stimul*. 2016;9:641–61.
73. Farahani F, Khadka N, Parra LC, Bikson M, Vöröslakos M. Transcranial electric stimulation modulates firing rate at clinically relevant intensities. *Brain Stimul*. 2024;17:561–71.
74. Greengrass PM, Tonge SR. Changes in brain monoamine concentrations during the oestrous cycle in the mouse: possible pharmacological implications. *J Pharm Pharmacol*. 1971;23:897–8.
75. Dazzi L, Seu E, Cherchi G, Barbieri PP, Matzeu A, Biggio G. Estrous Cycle-Dependent Changes in Basal and Ethanol-Induced Activity of Cortical Dopaminergic Neurons in the Rat. *Neuropsychopharmacol*. 2007;32:892–901.
76. Vandegriff BJ, You C, Satta R, Brodie MS, Lasek AW. Estradiol increases the sensitivity of ventral tegmental area dopamine neurons to dopamine and ethanol. *Ryabiniin AE, editor. PLoS ONE*. 2017;12:e0187698.
77. Ting JT, Lee BR, Chong P, Soler-Llavina G, Cobbs C, Koch C, et al. Preparation of acute brain slices using an optimized N-Methyl-D-glucamine protective recovery method. *J Vis Exp*. 2018;132:53825. <https://doi.org/10.37971/53825>.
78. Friard O, Gamba M. BORIS: a free, versatile open-source event-logging software for video/audio coding and live observations. *Methods Ecol Evol*. 2016;7:1325–30.
79. Krashia P, Cordella A, Nobili A, La Barbera L, Federici M, Leuti A, et al. Blunting neuroinflammation with resolvin D1 prevents early pathology in a rat model of Parkinson's disease. *Nat Commun*. 2019;10:3945.
80. Kempadoo KA, Mosharov EV, Choi SJ, Sulzer D, Kandel ER. Dopamine release from the locus coeruleus to the dorsal hippocampus promotes spatial learning and memory. *Proc Natl Acad Sci USA*. 2016;113:14835–40.
81. Šimić G, Babić Leko M, Wray S, Harrington CR, Delalle I, Jovanov-Milošević N, et al. Monoaminergic neuropathology in Alzheimer's disease. *Prog Neurobiol*. 2017;151:101–38.
82. Takeuchi T, Duszkievicz AJ, Sonneborn A, Spooner PA, Yamasaki M, Watanabe M, et al. Locus coeruleus and dopaminergic consolidation of everyday memory. *Nature*. 2016;537:357–62.
83. Broussard JI, Yang K, Levine AT, Tsetsenis T, Jensen D, Cao F, et al. Dopamine Regulates Aversive Contextual Learning and Associated In Vivo Synaptic Plasticity in the Hippocampus. *Cell Rep*. 2016;14:1930–9.
84. Mamad O, Stumpp L, McNamara HM, Ramakrishnan C, Deisseroth K, Reilly RB, et al. Place field assembly distribution encodes preferred locations. *PLoS Biol*. 2017;15:e2002365.
85. McNamara CG, Tejero-Cantero Á, Trouche S, Campo-Urriza N, Dupret D. Dopaminergic neurons promote hippocampal reactivation and spatial memory persistence. *Nat Neurosci*. 2014;17:1658–60.
86. Rossato JI, Bevilacqua LRM, Izquierdo I, Medina JH, Cammarota M. Dopamine controls persistence of long-term memory storage. *Science*. 2009;325:1017–20.
87. Corsetti V, Borreca A, Latina V, Giacovazzo G, Pignataro A, Krashia P, et al. Passive immunotherapy for N-truncated tau ameliorates the cognitive deficits in two mouse Alzheimer's disease models. *Brain Commun*. 2020;2:1–34.
88. Tagliatalata G, Hogan D, Zhang W-R, Dineley KT. Intermediate- and Long-Term Recognition Memory Deficits in Tg2576 Mice Are Reversed with Acute Calcineurin Inhibition. *Behav Brain Res*. 2009;200:95–9.
89. Mocellin P, Barnstedt O, Luxem K, Kaneko H, Wieweg S, Henschke JU, et al. A septal-ventral tegmental area circuit drives exploratory behavior. *Neuron*. 2024;112:1020–1032.e7.
90. Gil-Bea FJ, Aisa B, Schliebs R, Ramírez MJ. Increase of locomotor activity underlying the behavioral disinhibition in tg2576 mice. *Behav Neurosci*. 2007;121:340–4.
91. Luo Y-P, Liu Z, Wang C, Yang X-F, Wu X-Y, Tian X-L, et al. Anodal transcranial direct current stimulation alleviates cognitive impairment in an APP/PS1 model of Alzheimer's disease in the preclinical stage. *Neural Regen Res*. 2022;17:2278.
92. Kim W-I, Han J-Y, Song M-K, Park H-K, Jo J. Cognitive Function Improvement in Mouse Model of Alzheimer's Disease Following Transcranial Direct Current Stimulation. *Brain Sci*. 2020;10:547.
93. Duan M, Meng Z, Yuan D, Zhang Y, Tang T, Chen Z, et al. Anodal and cathodal transcranial direct current stimulations of prefrontal cortex in a rodent model of Alzheimer's disease. *Front Aging Neurosci*. 2022;14. Available from: <https://www.frontiersin.org/journals/aging-neuroscience/articles/10.3389/fnagi.2022.968451/full>. Cited 2025 Jan 31.
94. Carr DB, Sesack SR. Projections from the rat prefrontal cortex to the ventral tegmental area: target specificity in the synaptic associations with mesoaccumbens and mesocortical neurons. *J Neurosci*. 2000;20:3864–73.
95. Carr DB, Sesack SR. Terminals from the rat prefrontal cortex synapse on mesoaccumbens VTA neurons. *Ann N Y Acad Sci*. 1999;877:676–8.
96. Tzschenke TM, Schmidt WJ. Functional relationship among medial prefrontal cortex, nucleus accumbens, and ventral tegmental area in locomotion and reward. *Crit Rev Neurobiol*. 2000;14:131–42.

97. Frankle WG, Laruelle M, Haber SN. Prefrontal cortical projections to the midbrain in primates: evidence for a sparse connection. *Neuropsychopharmacology*. 2006;31:1627–36.
98. Tsetsenis T, Badya JK, Wilson JA, Zhang X, Krizman EN, Subramanian M, et al. Midbrain dopaminergic innervation of the hippocampus is sufficient to modulate formation of aversive memories. *Proc Natl Acad Sci USA*. 2021;118:e2111069118.
99. Frey U, Matthies H, Reymann KG, Matthies H. The effect of dopaminergic D1 receptor blockade during tetanization on the expression of long-term potentiation in the rat CA1 region in vitro. *Neurosci Lett*. 1991;129:111–4.
100. Lemon N, Manahan-Vaughan D. Dopamine D1/D5 receptors gate the acquisition of novel information through hippocampal long-term potentiation and long-term depression. *J Neurosci*. 2006;26:7723–9.
101. Cavaleiro C, Martins J, Gonçalves J, Castelo-Branco M. Memory and Cognition-Related Neuroplasticity Enhancement by Transcranial Direct Current Stimulation in Rodents: A Systematic Review. *Neural Plast*. 2020;2020:4795267.
102. Kronberg G, Bridi M, Abel T, Bikson M, Parra LC. Direct Current Stimulation Modulates LTP and LTD: Activity Dependence and Dendritic Effects. *Brain Stimul*. 2017;10:51–8.
103. Saxena V, Pal A. Role of Transcranial Direct Current Stimulation in the Management of Alzheimer's Disease: A Meta-analysis of Effects, Adherence and Adverse Effects. *Clin Psychopharmacol Neurosci*. 2021;19:589–99.
104. Yang H, de Jong JW, Tak Y, Peck J, Bateup HS, Lammel S. Nucleus Accumbens Subnuclei Regulate Motivated Behavior via Direct Inhibition and Disinhibition of VTA Dopamine Subpopulations. *Neuron*. 2018;97:434–449.e4.
105. Dunlop BW, Nemeroff CB. The role of dopamine in the pathophysiology of depression. *Arch Gen Psychiatry*. 2007;64:327–37.
106. Salamone JD, Pardo M, Yohn SE, López-Cruz L, SanMiguel N, Correa M. Mesolimbic Dopamine and the Regulation of Motivated Behavior. *Curr Top Behav Neurosci*. 2016;27:231–57.
107. Rueger MA, Keuters MH, Walberer M, Braun R, Klein R, Sparing R, et al. Multi-session transcranial direct current stimulation (tDCS) elicits inflammatory and regenerative processes in the rat brain. *PLoS ONE*. 2012;7:e43776.
108. Sevigny J, Chiao P, Bussière T, Weinreb PH, Williams L, Maier M, et al. The antibody aducanumab reduces A $\beta$  plaques in Alzheimer's disease. *Nature*. 2016;537:50–6.
109. van Dyck CH, Swanson CJ, Aisen P, Bateman RJ, Chen C, Gee M, et al. Lecanemab in Early Alzheimer's Disease. *N Engl J Med*. 2023;388:9–21.
110. Panza F, Lozupone M, Logroscino G, Imbimbo BP. A critical appraisal of amyloid- $\beta$ -targeting therapies for Alzheimer disease. *Nat Rev Neurol*. 2019;15:73–88.
111. Salloway S, Chalkias S, Barkhof F, Burkett P, Barakos J, Purcell D, et al. Amyloid-Related Imaging Abnormalities in 2 Phase 3 Studies Evaluating Aducanumab in Patients With Early Alzheimer Disease. *JAMA Neurol*. 2022;79:13–21.
112. Golde TE. Disease-Modifying Therapies for Alzheimer's Disease: More Questions than Answers. *Neurotherapeutics*. 2022;19:209–27.
113. Pittcock RR, Aakre JA, Castillo AM, Ramanan VK, Kremers WK, Jack CR, et al. Eligibility for Anti-Amyloid Treatment in a Population-Based Study of Cognitive Aging. *Neurology*. 2023;101:e1837–49.
114. Hampel H, Elhage A, Cho M, Apostolova LG, Nicoll JAR, Atri A. Amyloid-related imaging abnormalities (ARIA): radiological, biological and clinical characteristics. *Brain*. 2023;146:4414–24.

## Publisher's Note

Springer Nature remains neutral with regard to jurisdictional claims in published maps and institutional affiliations.